

Effects of Strong Electronic Coupling in Chlorin and Bacteriochlorin Dyads

Hyun Suk Kang,[†] Nopondo N. Esemoto,[‡] James R. Diers,[§] Dariusz M. Niedzwiedzki,[#] Jordan A. Greco,^{||} Joshua Akhigbe,[‡] Zhanqian Yu,[‡] Chirag Pancholi,[‡] Ganga Viswanathan Bhagavathy,[‡] Jamie K. Nguyen,[‡] Christine Kirmaier,[†] Robert R. Birge,^{*||} Marcin Ptaszek,^{*,‡} Dewey Holten,^{*,†} and David F. Bocian^{*,§}

[†]Department of Chemistry, Washington University, St. Louis, Missouri 63130-4889, United States

[‡]Department of Chemistry and Biochemistry, University of Maryland, Baltimore County, Baltimore, Maryland 21250-0001, United States

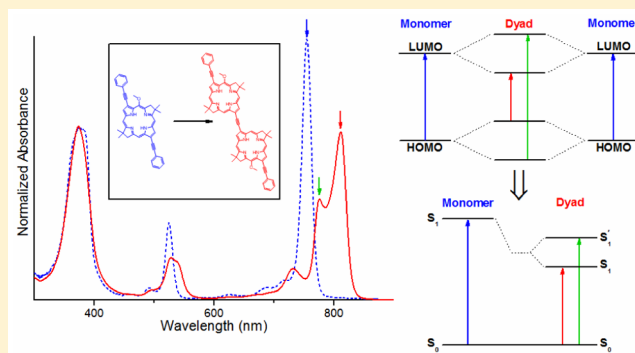
[§]Department of Chemistry, University of California, Riverside, California 92521-0403, United States

[#]Photosynthetic Antenna Research Center, Washington University, St. Louis, Missouri 63130-4889, United States

^{||}Department of Chemistry, University of Connecticut, Storrs, Connecticut 06269-3060, United States

Supporting Information

ABSTRACT: Achieving tunable, intense near-infrared absorption in molecular architectures with properties suitable for solar light harvesting and biomedical studies is of fundamental interest. Herein, we report the photophysical, redox, and molecular-orbital characteristics of nine hydroporphyrin dyads and associated benchmark monomers that have been designed and synthesized to attain enhanced light harvesting. Each dyad contains two identical hydroporphyrins (chlorin or bacteriochlorin) connected by a linker (ethynyl or butadiynyl) at the macrocycle β -pyrrole (3- or 13-) or *meso* (15-) positions. The strong electronic communication between constituent chromophores is indicated by the doubling of prominent absorption features, split redox waves, and paired linear combinations of frontier molecular orbitals. Relative to the benchmarks, the chlorin dyads in toluene show substantial bathochromic shifts of the long-wavelength absorption band (17–31 nm), modestly reduced singlet excited-state lifetimes ($\tau_S = 3.6$ –6.2 ns vs 8.8–12.3 ns), and increased fluorescence quantum yields ($\Phi_f = 0.37$ –0.57 vs 0.34–0.39). The bacteriochlorin dyads in toluene show significant bathochromic shifts (25–57 nm) and modestly reduced τ_S (1.6–3.4 ns vs 3.5–5.3 ns) and Φ_f (0.09–0.19 vs 0.17–0.21) values. The τ_S and Φ_f values for the bacteriochlorin dyads are reduced substantially (up to ~20-fold) in benzonitrile. The quenching is due primarily to the increased $S_1 \rightarrow S_0$ internal conversion that is likely induced by increased contribution of charge-resonance configurations to the S_1 excited state in the polar medium. The fundamental insights gained into the physicochemical properties of the strongly coupled hydroporphyrin dyads may aid their utilization in solar-energy conversion and photomedicine.



1. INTRODUCTION

A goal of research on molecular light-harvesting systems is to extend photon absorption deeply into the near-infrared (NIR) region, which contains over half of the solar radiation reaching Earth.¹ Nature's photosynthetic antenna pigments are bacteriochlorins and chlorins, which have two or one reduced pyrrole rings, compared to no reduced rings for porphyrins.² The long-wavelength absorption band of bacteriochlorins, chlorins, and porphyrins are, respectively, intense and in the NIR, strong and in the red, or weak and in the visible. Due to chemical stability and ease of synthesis, porphyrinic pigments and associated multichromophore arrays have been extensively investigated.^{3–7} The stability of chlorins and bacteriochlorins prepared by *de novo* synthetic strategies has been enhanced by the incorporation of geminal methyl groups at the 18-position of the former or 8,18-

positions of the latter. These groups together with diverse auxochromic macrocycle substituents and macrocycle variations (e.g., incorporation of fused rings) have produced sets of stable, synthetic chlorins and bacteriochlorins with tunable red and NIR absorption bands that span the region from ~600 to ~900 nm in small increments.^{8–12}

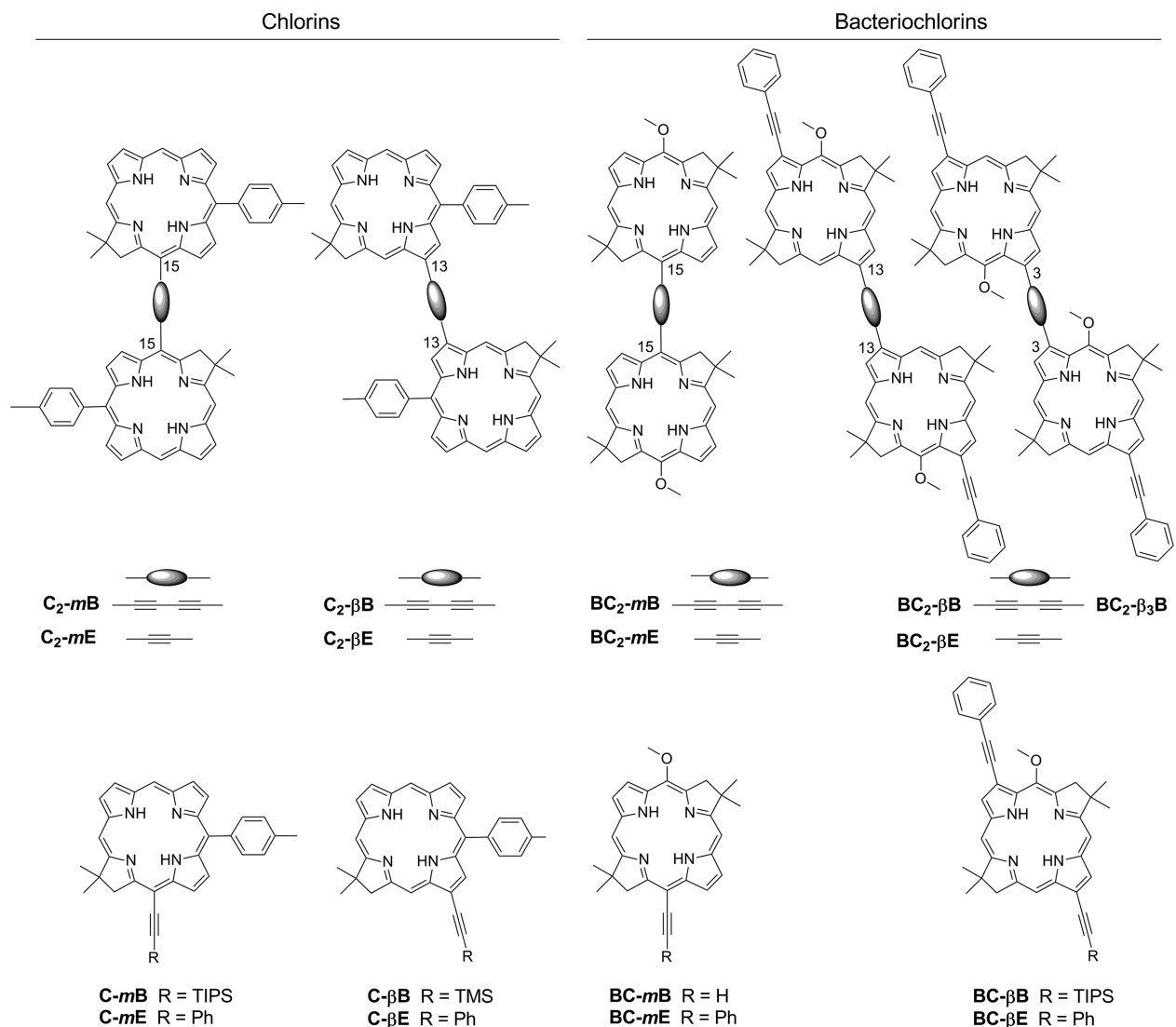
The construction of tetrapyrrole dyads (and larger arrays) with strong linker-mediated electronic interactions between constituent macrocycles has been employed as another means to extend absorption deeper into the NIR region. This strategy has been developed by Therien and co-workers^{13–20} and Anderson and

Received: November 1, 2015

Revised: December 21, 2015

Published: January 14, 2016

Chart 1. Molecular Structures of Hydroporphyrin Dyads and Benchmarks



co-workers^{21–28} using porphyrins joined by conjugating linkers such as ethynyl and butadiynyl groups. Linker-mediated electronic mixing of frontier molecular orbitals (MOs) of the constituents leads to electron delocalization over the entire array. Such mixing for porphyrin arrays is generally accompanied by a reduction in the energy gap between lowest unoccupied and highest occupied MOs, the LUMO–HOMO gap. Because the HOMO → LUMO electronic configuration makes a significant contribution to the nature of the lowest singlet excited state (S_1), the diminished MO energy gap in turn underlies an associated bathochromic shift in the long-wavelength ($S_0 \rightarrow S_1$) absorption band. The relationship between chemical structure (linker identity and attachment sites, nonlinking macrocycle subunits, number of subunits, and central metal ion) and the absorption/emission,^{14,17} redox,²⁰ and excited-state characteristics (e.g., lifetime and fluorescence yield)^{15,26} have been systematically studied for multiporphyrin arrays. In some cases, the desired bathochromic (and hyperchromic) absorption shift is accompanied by unfavorable changes in other properties, such as reduced excited-state lifetime.¹⁶

Although chlorin/bacteriochlorin monomers by nature have modest/strong absorption in the red/NIR regions, the strategy to extend the spectral range to longer wavelengths *via* strong

interchromophore electronic coupling has been explored far less extensively for these pigments than for porphyrins. There have been studies of chlorin–chlorin dyads,^{29–33} chlorin–bacteriochlorin dyads,^{34,35} bacteriochlorin arrays,³⁶ and recently a few pairs of strongly coupled chlorin–chlorin and bacteriochlorin–bacteriochlorin dyads.³⁷ The *de novo* synthetic methodology employed for the latter pairs of arrays opens the door to variations in conjugated linkers, macrocycle–linker connection motifs, and substituent patterns (to further tune properties) around the chlorin or bacteriochlorin units. However, systematic studies of the relationship between chemical composition, electronic structure, and physicochemical properties of such strongly coupled hydroporphyrin arrays have not been performed. A recent computational study affords insights into the MO properties of such bacteriochlorin–bacteriochlorin dyads as a function of the torsional angle between the constituents and the potential effects on the optical spectra.³⁸

The present paper explores in detail the connections between the photophysical, redox, and MO properties of several sets of chlorin–chlorin and bacteriochlorin–bacteriochlorin dyads (Chart 1). The two chlorin (C) or bacteriochlorin (BC) constituents are joined by an ethyne (E) or butadiyne (B) linker at the macrocycle β -pyrrole (3- or 13-) or *meso*-bridge (15-)

positions. Several of the dyads (and benchmark monomers) have been synthesized previously, and preliminary photophysical studies have been performed.³⁷ The S_1 excited-state properties (decay pathway yields and rate constants) of those arrays have been characterized herein. Additionally, new pairs of dyads and associated benchmarks have been prepared and studied for the first time. The experimental studies employ static and time-resolved optical spectroscopy and electrochemistry, with analysis of the results supported by MO characteristics derived from density functional theory (DFT) calculations. The combined findings give fundamental insights into how strong linker-mediated electronic coupling impacts the electronic properties of hydroporphyrin dyads.

2. EXPERIMENTAL SECTION

2.1. Synthesis. Two chlorin dyads (C_2 - β B and C_2 - β E) and benchmarks (C - β B and C - β E) and bacteriochlorin dyads (BC_2 - β B, BC_2 - β E, and BC_2 - m B) and benchmarks (BC - β B, BC - β E, and BC - m B) were synthesized previously.³⁷ The syntheses of new chlorin dyads (C_2 - m B and C_2 - m E) and benchmarks (C - m B and C - m E) and new bacteriochlorin dyads (BC_2 - m E and BC_2 - β_3 B) and benchmark (BC - m E) are described in the following sections with details in the [Supporting Information](#).

2.2. Photophysical Properties. All photophysical measurements were performed on dilute (μ M) solutions in toluene or benzonitrile at room temperature. Static absorption spectra were acquired using a Shimadzu UV-1800 spectrometer, and static emission studies utilized a Horiba Nanolog spectrofluorometer. Samples were Ar-purged for determination of the singlet excited-state (S_1) lifetime (τ_S), $S_1 \rightarrow S_0$ fluorescence quantum yield (Φ_f), and yield of intersystem crossing (Φ_{isc}) from S_1 to the lowest triplet excited state (T_1), i.e., the triplet yield. The Φ_f measurements used samples with $A \leq 0.1$ at the 500–550 nm excitation wavelength and *meso*-tetraphenylporphyrin in non-degassed toluene ($\Phi_f = 0.070$ ¹²) as the standard. Transient absorption studies (e.g., to obtain τ_S and Φ_{isc}) employed attenuated (0.5–1 μ J) \sim 100 fs excitation flashes (typically at the long-wavelength absorption maximum) from a 1 kHz Ti:sapphire laser system with optical parametric amplifier (Spectra Physics). Measurements employed two transient-absorption setups (Ultrafast Systems): One instrument (Helios) with \sim 100 fs white-light probe pulses and an optical pump–probe delay up to \sim 8 ns was used for samples with $\tau_S \leq 1$ ns. A second spectrometer (EOS) with \sim 1 ns probe pulses and detection in 0.1 ns bins for times to 0.5 ms was additionally used for samples with $\tau_S > 1$ ns. The Φ_{isc} values were obtained by comparing the extent of ground-state bleaching due to S_1 at early times to that for T_1 at the asymptote of the S_1 decay, both referenced to the flanking relatively featureless excited-state absorption.

2.3. Electrochemistry. Electrochemical studies were performed using a standard three-electrode cell, as described previously.³⁹

2.4. Computational Calculations. DFT calculations were performed on all the monomers and dyads with Spartan¹⁰ for Windows (Wavefunction, Inc., Irvine, CA) using the B3LYP functional and 6-31G* basis set in vacuum.⁴⁰ Calculations for monomers substituted with triisopropylsilyl (TIPS)-ethynyl were performed on the trimethylsilyl (TMS)-ethynyl analogue. Full structure geometry optimization was performed for each run. For the dyads, several geometries with different torsional angles (about the linker) between the macrocycles were examined to ensure location of the conformation corresponding to the global energy minimum. The energies for conformations

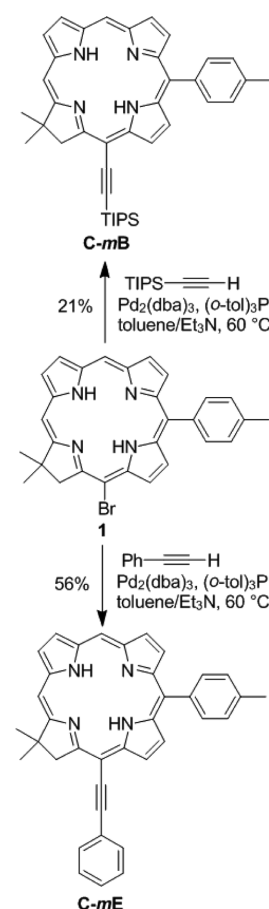
with different torsional angles between the macrocycles were computed by fixing the torsional angle at a specified value, followed by optimizing the geometry of the rest of the structure.

Resolution enhancement of the UV–vis–NIR spectra utilized a combination of Fourier-transform self-deconvolution, maximum-entropy linear prediction (LOMEP)^{41,42} and simple second and fourth derivative methods.^{43,44} The procedure was implemented in MathScriptor 3.7.2 (www.mathscriptor.org). Total and differential oscillator strengths were monitored to verify that the relative allowedness of the bands or band systems was retained.

3. RESULTS

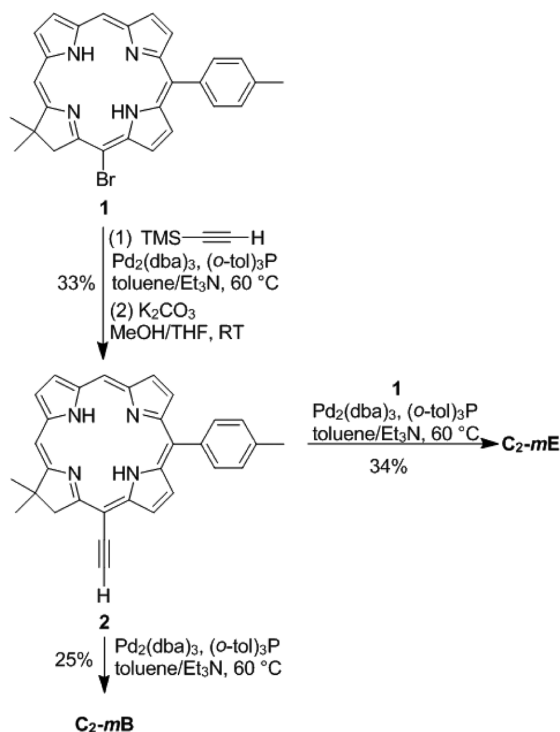
3.1. Synthesis. The new hydroporphyrin dyads and their benchmarks were prepared following a general strategy described previously.³⁷ The *meso*-linked chlorin dyads (C_2 - m B and C_2 - m E) and benchmark monomers (C - m E and C - m B) were synthesized starting from known 15-bromochlorin **1**⁴⁵ (Schemes 1 and 2).

Scheme 1. Syntheses of **C**- m B and **C**- m E



Sonogashira reaction of **1** with triisopropylsilylacetylene (TIPS-acetylene), under reported conditions,⁴⁶ afforded **C**- m B (21% yield) after an extensive purification, which includes preparative thin-layer chromatography (TLC). Subsequent cleavage of the TIPS group using tetra-*n*-butylammonium fluoride (TBAF)/tetrahydrofuran (THF) provides **2** in 27% only. The yield of **2** in this case was diminished by extensive decomposition of chlorin upon treatment with TBAF.

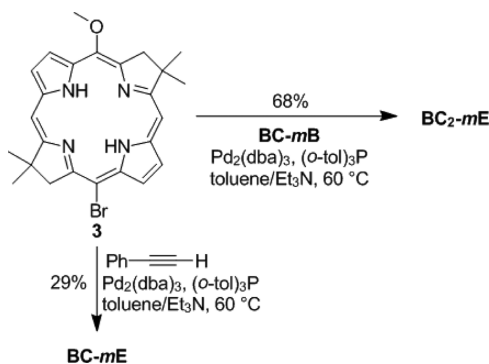
Given the low yield and difficulties with purification of **C**- m B and low yield of its deprotection, an alternate synthesis of **2** *via*

Scheme 2. Syntheses of C_2 -*mB* and C_2 -*mE*

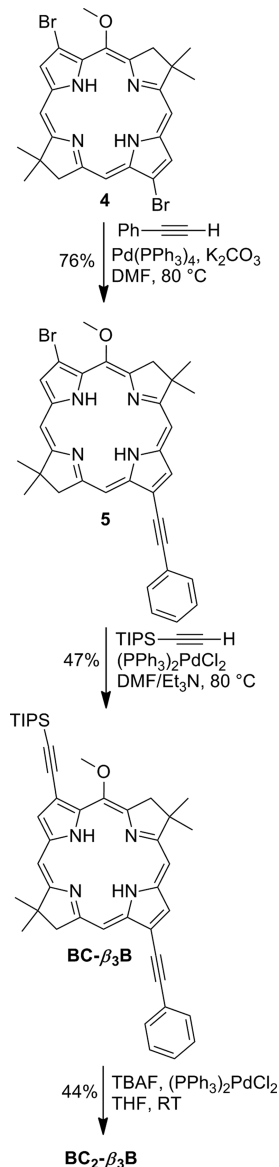
the corresponding 15-trimethylsilylchlorin (TMS-ethynylchlorin) was pursued. Sonogashira reaction of **1** with TMS-acetylene, under reported conditions,⁴⁶ provides a complex mixture of side-products, and isolation and purification of the desired product requires several column chromatography separations and finally preparative TLC. Therefore, the semipurified TMS-ethynylchlorin was subjected to a deprotection reaction (K₂CO₃, MeOH/THF), and the final product (**2**) was obtained in 33% overall yield for the two steps (Sonogashira reaction and deprotection).

Homocoupling of **2** under previously reported conditions³⁷ afforded butadiyne-linked dyad **C₂-mB** in 25% yield, while Sonogashira reaction of **2** with **1** afforded ethynyl-linked dyad **C₂-mE** in 34% yield (Scheme 2). Benchmark monomer **C-mE** was obtained in Sonogashira reaction of **1** with phenylacetylene, in 56% yield (Scheme 1).

The *meso*-linked bacteriochlorin dyad **BC₂-mE** was synthesized in a Sonogashira reaction of known 15-acetylene-substituted bacteriochlorin **BC-mB**³⁷ with 15-bromobacteriochlorin **3**⁴⁷ in 68% yield (Scheme 3). The corresponding

Scheme 3. Syntheses of **BC-mE** and **BC₂-mE**

benchmark monomer **BC-mE** was prepared in Sonogashira reaction of **3** with phenylacetylene, in 29% yield (Scheme 3). The 3–3'-linked dyad **BC₂-β₃B** was prepared in sequential palladium-catalyzed cross-coupling reactions, starting from known dibromobacteriochlorin **4**⁴⁷ (Scheme 4). Thus, following a

Scheme 4. Synthesis of **BC₂-β₃B**

reported protocol for synthesis of nonsymmetrically substituted bacteriochlorins,⁴⁸ Sonogashira reaction of **4** with phenylacetylene afforded selectively monosubstituted bacteriochlorin **5** in 76% yield. Subsequent Sonogashira reaction of **5** with TIPS-protected acetylene provided nonsymmetrically substituted bacteriochlorin **BC-β₃B** in 47% yield. Monomer **BC-β₃B** was *in situ* deprotected (using TBAF), and homocoupling of resulting acetylene-substituted bacteriochlorin under reported conditions³⁷ provided **BC₂-β₃B** in 44% yield.

3.2. Electronic Ground-State Absorption Spectra. Figure 1 shows the ground-state absorption spectra of the chlorin (A–D) and bacteriochlorin (E–H) dyads (solid red) and benchmarks (solid blue) in toluene. The spectra are normalized to total intensity obtained by integration of spectra (300–1000

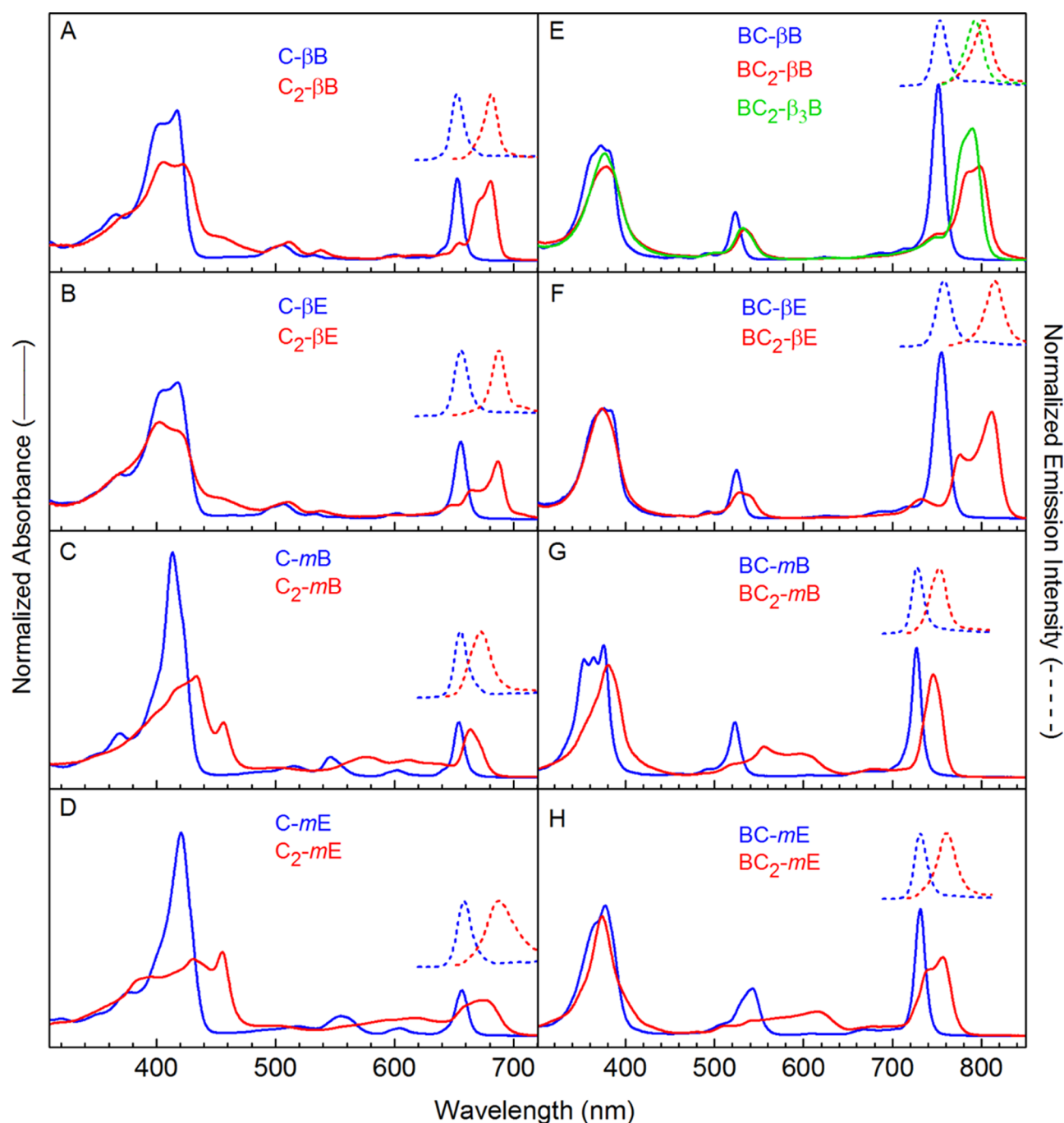


Figure 1. Absorption (solid) and fluorescence spectra (dashed) of the chlorin (left) and the bacteriochlorin (right) benchmarks (blue) and dyads (red and green) in toluene. Absorption spectra were normalized to the total integrated intensity (300–1000 nm for spectra plotted vs cm^{-1}), and all fluorescence spectra (500–550 excitation) were normalized to the peak intensity.

nm) plotted in wavenumbers (cm^{-1}). This procedure is useful for comparing relative spectral intensities for sets of tetrapyrroles.¹² Similar spectra are observed in benzonitrile, except for small differences in peak positions and intensity ratios (Figure S1 and Table S1). Inspection of Figures 1 and S1 show that the spectra, particularly for the dyads, are rich with features that may be partially overlapped depending on the spectral region and compound. Resolution enhancement (rather than simple curve fitting) was employed to obtain better estimates for the wavelength maxima of the underlying bands (Figure S2); the peak positions obtained thereby are listed in Table 1. The key

results and conclusions do not depend on exact wavelength maxima.

The absorption spectra of the benchmarks show the features expected for chlorin and bacteriochlorin monomers. These features are the near-UV (NUV) Soret (B_y , B_x) bands, the weak green–orange Q_x band, and the red/NIR Q_y band. [The Q_x and Q_y designations may be reversed for chlorin *C-mE* due to the effect of the *meso*-ethyne group on the ordering of the two highest-filled MOs.^{34,49}] Each of these origin features has at least one vibronic satellite to higher energy. Normally B_y lies at higher energy than B_x for the bacteriochlorins. Depending on the macrocycle and substituent pattern, bands in the Soret region are

Table 1. Spectral Characteristics of Hydroporphyrin Dyads and Benchmarks in Toluene^a

cmpd	λ_B (nm)	λ_{Q_2} (nm)	$\Delta\lambda_{Q_2}^{\text{shift}}$ (cm ⁻¹)	$\Delta\lambda_{Q_2}^{\text{split}}$ (cm ⁻¹)	λ_{Q_1} (nm)	$\Delta\lambda_{Q_1}^{\text{shift}}$ (cm ⁻¹)	$\Delta\lambda_{Q_1}^{\text{split}}$ (cm ⁻¹)	λ_{em} (nm)	fwhm em (nm)
Chlorins									
C- β B	401, 417	532			652			652	13
C ₂ - β B	422, 452	538	210	<40	672, 681	653	197	681	13
C- β E	403, 418	533			656			656	13
C ₂ - β E	417, 452	538	174	<40	664, 687	688	504	687	13
C- <i>m</i> B	414, 423 ^b	546			654			655	13
C ₂ - <i>m</i> B	434, 457	578, 612	1975	961	663, 671	387	180	673	21
C- <i>m</i> E	421, 429 ^b	555			656			658	13
C ₂ - <i>m</i> E	430, 455	594, 620	1889	706	668, 680	538	264	689	30
Bacteriochlorins									
BC- β B	379	523			752			753	18
BC ₂ - β B	378	532	323	<40	783, 801	813	287	802	23
BC ₂ - β_3 B	377	531	288	<40	780, 790	640	162	795	23
BC- β E	382	525			755			758	19
BC ₂ - β E	373	526, 540	529	493	775, 812	930	588	815	24
BC- <i>m</i> B	375	523			727			728	15
BC ₂ - <i>m</i> B	380	557, 597	2370	1203	746, 750	422	71	753	22
BC- <i>m</i> E	377	542			731			733	15
BC ₂ - <i>m</i> E	373	578, 616	2216	1067	738, 758	487	358	763	24

^aThe absorption bands of the benchmark monomers are listed as B, Q₂, and Q₁ bands. For all the monomers, except C-*m*E, the Q₂ band is Q_x and Q₁ is Q_y. The assignment is reversed for C-*m*E. Columns $\Delta\lambda_{Q_1}^{\text{shift}}$ and $\Delta\lambda_{Q_2}^{\text{shift}}$ give the shift in position of the respective Q_x band of the dyad versus Q_x of the monomer. Columns $\Delta\lambda_{Q_1}^{\text{split}}$ and $\Delta\lambda_{Q_2}^{\text{split}}$ give the splitting of the respective Q_β and Q_α pair of bands of the dyad. ^bShoulder on the main feature.

substantially overlapped and may contain contributions from transitions in addition to B_y and B_x.^{50–53} The variable spectral overlap can be seen in the NUV spectra for the four chlorin monomers in Figure 1A–D. Two partially resolved features of comparable amplitude are found for C- β B and C- β E (at 401–404 nm and 417–418 nm, respectively; Table 1). However, the overall Soret contour is much narrower for C-*m*B and C-*m*E with net peak intensity much greater relative to Q₂ than for C- β B and C- β E. The differences likely reflect greater overlap and perhaps a greater disparity of relative B_y and B_x intensities for the two meso-substituted chlorins, with the weaker member at longer wavelength than the stronger for C-*m*B (Figure 1C). Less variation in Soret profile is observed among the four bacteriochlorin benchmarks (Figure 1E–H). The Soret has lost considerable intensity at the expense of Q₂ (and to a lesser extent Q_x) for bacteriochlorin versus chlorin benchmarks, due to macrocycle-induced differences in energy gaps between frontier MOs as expected within the four-orbital model (*vide infra*).^{3,50,51}

The strong electronic interactions between constituents in the dyads (and potential rotations in optical axes) renders simple B_y, B_x, Q_x, and Q_y assignments misleading. However, although there are spectral shifts/splittings and changes in relative intensities, the absorption spectra of the dyads (Figure 1, solid red) have main features in the same regions as the monomers (solid blue). Thus, to simplify discussion, it is convenient to denote the absorption manifolds of the dyads as B, Q₂, and Q₁, progressing from higher to lower energy. Additionally, prominent splitting of bands for dyads versus monomers is observed. The higher-energy and lower-energy members of a split pair will be denoted β and α , respectively. For example, Q_x for a monomer may give the split pair Q_{2 β} and Q_{2 α} in the visible region for a dyad. Similarly, Q_y for a monomer may give the split pair Q_{1 β} and Q_{1 α} in the red or NIR for a dyad.

The hydroporphyrin dyads all show a significant bathochromic shift and splitting (and perhaps broadening) in the lowest absorption manifold relative to the benchmarks. The shift between the Q₂ band of the benchmark and the Q_{1 α} band of the

dyad (the lowest-energy feature in each case) is designated $\Delta\lambda_{Q_1}^{\text{shift}}$, and the splitting between the Q_{1 β} and Q_{1 α} bands of the dyad is denoted $\Delta\lambda_{Q_1}^{\text{split}}$. The values (in cm⁻¹) are listed in Table 1. For example, of the nine dyads, chlorin C₂-*m*B shows the smallest shift (654 → 671 nm; 387 cm⁻¹) and split (663 ↔ 671 nm; 180 cm⁻¹), while bacteriochlorin BC₂- β E has the largest shift (755 → 812 nm; 930 cm⁻¹) and split (775 ↔ 812 nm; 588 cm⁻¹).

For the four chlorin dyads, $\Delta\lambda_{Q_1}^{\text{shift}}$ (in cm⁻¹) increases in the order C₂-*m*B (387) < C₂-*m*E (538) < C₂- β B (653) < C₂- β E (688), while $\Delta\lambda_{Q_1}^{\text{split}}$ increases in the order C₂-*m*B (180) < C₂- β B (197) < C₂-*m*E (264) < C₂- β E (504). The smallest shift and split both occur for C₂-*m*B, and the largest pair of values occur for C₂- β E. Dyads C₂-*m*E and C₂- β B show intermediate values but with reversed order of split and shift.

Identical trends are found for the corresponding bacteriochlorin dyads, supplemented by BC₂- β_3 B, which has a butadiyne linker at the 3- rather than 13-position. The $\Delta\lambda_{Q_1}^{\text{shift}}$ values (in cm⁻¹) increase in the order BC₂-*m*B (422) < BC₂-*m*E (487) < BC₂- β_3 B (640) < BC₂- β B (813) < BC₂- β E (930), while $\Delta\lambda_{Q_1}^{\text{split}}$ increases in the order BC₂-*m*B (71) < BC₂- β_3 B (162) < BC₂- β B (287) < BC₂-*m*E (358) < BC₂- β E (588). Again, BC₂-*m*B exhibits the smallest shift and split, with BC₂- β E being the largest and BC₂-*m*E and BC₂- β B being intermediate with reversed split and shift order. Attachment of the butadiynyl linker at the 3-position (BC₂- β_3 B) versus the 13-position (BC₂- β B) affords a smaller shift (640 vs 813 cm⁻¹) and split (162 vs 287 cm⁻¹). Analysis of the resolution-enhanced spectra (Figure S2) suggests that the first vibronic satellite associated with the Q_{1 α} origin band lies to higher energy by ~600–1100 cm⁻¹ for the bacteriochlorin and chlorin dyads.

The visible region (~500–650 nm) of the β -linked chlorin dyads (C₂- β B and C₂- β E) and bacteriochlorin dyads (BC₂- β B, BC₂- β E, and BC₂- β_3 B) reveals no clear splitting within the Q₂ manifold and only modest (5–9 nm; ~170–320 cm⁻¹) shifts from the Q_x bands of the benchmarks. The shifts/splittings are roughly one-third the size of those observed in the red/NIR Q₁ (Q_y of monomers) manifold. Substantially larger bathochromic

Table 2. Singlet Excited-State Properties of Chlorins

compd	solvent	τ_S (ns)	Φ_f	Φ_{isc}	Φ_{ic}	$(k_f)^{-1}$ (ns)	$(k_{isc})^{-1}$ (ns)	$(k_{ic})^{-1}$ (ns)
C- β B	toluene	9.3	0.34	0.50	0.16	27	19	58
	benzonitrile	9.1	0.31	0.50	0.19	29	18	48
C ₂ - β B	toluene	5.7	0.57	0.29	0.14	10	20	41
	benzonitrile	5.0	0.52	0.25	0.23	9.6	20	22
C- β E	toluene	8.8	0.39	0.55	0.060	23	16	147
	benzonitrile	8.5	0.36	0.48	0.16	24	18	53
C ₂ - β E	toluene	5.2	0.48	0.25	0.27	11	21	19
	benzonitrile	4.8	0.40	0.30	0.30	12	16	16
C- <i>m</i> B	toluene	11.5	0.36	0.57	0.070	32	20	164
	benzonitrile	11.4	0.34	0.57	0.090	34	20	127
C ₂ - <i>m</i> B	toluene	6.2	0.45	0.37	0.18	14	17	34
	benzonitrile	2.9	0.24	0.17	0.59	12	17	5.0
C- <i>m</i> E	toluene	12.3	0.38	0.53	0.090	32	23	137
	benzonitrile	12.3	0.37	0.54	0.090	33	23	137
C ₂ - <i>m</i> E	toluene	3.6	0.37	0.18	0.45	9.7	20	8.0
	benzonitrile	2.4	0.25	0.13	0.62	9.6	18	3.9

Table 3. Singlet Excited-State Properties of Bacteriochlorins

compd	solvent	τ_S (ns)	Φ_f	Φ_{isc}	Φ_{ic}	$(k_f)^{-1}$ (ns)	$(k_{isc})^{-1}$ (ns)	$(k_{ic})^{-1}$ (ns)
BC- β B	toluene	3.7	0.20	0.43	0.37	19	8.6	10
	benzonitrile	3.7	0.21	0.40	0.39	18	9.3	9.5
BC ₂ - β B	toluene	2.3	0.17	0.14	0.69	14	16	3.3
	benzonitrile	0.28	0.028	0.021	0.95	10	13	0.29
BC ₂ - β_3 B	toluene	2.4	0.18	0.17	0.65	13	14	3.7
	benzonitrile	0.30	0.022	0.010	0.97	14	30	0.31
BC- β E	toluene	3.5	0.21	0.36	0.43	17	9.7	8.1
	benzonitrile	3.4	0.22	0.37	0.41	15	9.2	8.3
BC ₂ - β E	toluene	2.1	0.19	0.17	0.64	11	12	3.3
	benzonitrile	0.31	0.028	0.022	0.95	11	14	0.33
BC- <i>m</i> B	toluene	4.9	0.17	0.56	0.27	29	8.8	18
	benzonitrile	5.0	0.18	0.56	0.26	28	8.9	19
BC ₂ - <i>m</i> B	toluene	3.4	0.18	0.39	0.43	19	8.7	7.9
	benzonitrile	0.12	0.008	0.008	0.98	15	15	0.12
BC- <i>m</i> E	toluene	5.3	0.17	0.50	0.33	31	11	16
	benzonitrile	5.3	0.16	0.52	0.32	33	10	17
BC ₂ - <i>m</i> E	toluene	1.6	0.091	0.090	0.82	18	18	2.0
	benzonitrile	0.23	0.005	0.032	0.96	46	7.2	0.24

shifts (~ 65 – 75 nm; ~ 2000 cm^{-1}) and splittings (~ 25 – 40 nm; ~ 700 – 1200 cm^{-1}) are found for the *meso*-linked chlorin dyads (C₂-*m*B and C₂-*m*E) and bacteriochlorin dyads (BC₂-*m*B and BC₂-*m*E). These shifts/splittings are roughly 4-fold greater than the (already substantial) effects observed in the lower-energy Q₁ manifold.

3.3. Fluorescence Spectra. Figure 1 shows room-temperature fluorescence spectra of the chlorin/bacteriochlorin dyads (dashed red) and their benchmarks (dashed blue) in toluene. The emission maximum and full-width-at-half-maximum (fwhm) of each compound are listed in Table 1. Similar spectra are observed in benzonitrile (Figure S1 and Table S1). The fluorescence of each dyad is bathochromically shifted from the benchmark in parallel with the above-noted shift in the position of the Q_{1 α} band of the dyad relative to the long-wavelength absorption band of the benchmark (Q_y, except for perhaps C-*m*E, as noted above). The (Stokes) shift between the fluorescence and corresponding absorption maximum is generally <5 nm. This finding suggests that there is minimal rearrangement of molecular structures of the dyads or reorientation of the solvent molecules in the excited versus ground states.

The fluorescence from each dyad is dominated by an apparent origin band, with much weaker vibronic components to longer wavelength that may be somewhat more structured for dyads with a *meso*- versus β -linker motif. The fluorescence of the dyads (unlike the benchmarks) is generally not in mirror symmetry to the long-wavelength (Q₁) absorption manifold. This finding indicates that the splitting of absorption bands (Q_{1 β} and Q_{1 α}) for the dyads relative to the benchmarks (generally Q_y) does not arise from vibronic satellites associated with a single electronic state but has other root origins including different electronic transitions (*vide infra*).

3.4. Singlet Excited-State Lifetime and Decay-Pathway Yields. Table 2 (chlorins) and Table 3 (bacteriochlorins) summarize the photophysical properties of the lowest singlet excited state (S₁) of the dyads and benchmarks. The measured values include the S₁ lifetime (τ_S) and the quantum yields for S₁ \rightarrow S₀ fluorescence (Φ_f) and S₁ \rightarrow T₁ intersystem crossing (Φ_{isc}). The values of Φ_f for the four chlorin dyads in toluene and the two β -linked members (C₂- β B and C₂- β E) in benzonitrile (0.37–0.57) are larger than those for the benchmarks (0.34–0.39), and the values of τ_S are smaller for the dyads (3.6–7.4 ns)

versus the benchmarks (8.8–12.3 ns). The Φ_f and τ_S for meso-linked chlorin dyads (C_2 -mB and C_2 -mE) are smaller in benzonitrile (0.24–0.25; 2.4–2.9 ns) than in toluene (0.37–0.45; 3.6–6.2 ns). The five bacteriochlorin dyads have Φ_f and τ_S in toluene (0.09–0.19; 1.6–3.4 ns) that are moderately smaller than those for the benchmarks in toluene (0.17–0.21; 3.5–5.5 ns) and that are substantially reduced in benzonitrile (0.005–0.028; 0.12–0.31 ns).

The Φ_{isc} values for all four chlorin dyads in toluene and C_2 - β B and C_2 - β E in benzonitrile (0.18–0.37) are smaller than those for the benchmarks (0.48–0.57). Chlorin dyads C_2 -mB and C_2 -mE have smaller Φ_{isc} in benzonitrile (0.13–0.17) than in toluene (0.18–0.37), whereas the values for the benchmarks are virtually the same in the two media (0.54–0.57 vs 0.53–0.57). The five bacteriochlorin dyads have Φ_{isc} substantially reduced in benzonitrile (0.008–0.032) compared to toluene (0.09–0.39), whereas the benchmarks are less solvent sensitive (0.26–0.43 vs 0.36–0.56).

The above-noted Φ_f and Φ_{isc} values afford the yield of the third S_1 decay pathway, $S_1 \rightarrow S_0$ internal conversion, by the simple calculation $\Phi_{ic} = 1 - \Phi_f - \Phi_{isc}$. The four chlorin dyads in toluene and C_2 - β B and C_2 - β E in benzonitrile have Φ_{ic} that are on the average larger (0.14–0.45) than those for the benchmarks (0.06–0.19). The companions C_2 -mB and C_2 -mE in benzonitrile have larger Φ_{ic} (0.59–0.62) than the benchmarks (0.09) in this solvent. The five bacteriochlorin dyads have a range of Φ_{ic} in toluene (0.43–0.82) that are elevated to near unity (0.95–0.98) in benzonitrile, whereas the values for the benchmarks are smaller and about the same in the two media (0.27–0.43 vs 0.26–0.41).

3.5. Rate Constants for Singlet Excited-State Decay Routes. The rate constants for the three S_1 decay pathways, $S_1 \rightarrow S_0$ fluorescence (k_f), $S_1 \rightarrow T_1$ intersystem crossing (k_{isc}), and $S_1 \rightarrow S_0$ internal conversion (k_{ic}), are obtained from the corresponding yields and the S_1 lifetime via the expression $k_i = \Phi_i/\tau_S$, where $i = f, isc, ic$. The values are listed in Table 2 (chlorins) and Table 3 (bacteriochlorins) as the corresponding time constant in units of nanoseconds.

The rate constant for fluorescence (k_f) is related to the rate constant for absorption via the Einstein coefficients.⁵⁴ This connection is illustrated in Figure 2 for the chlorins (A) and the bacteriochlorins (B), which plots k_f (in units of ns⁻¹) versus the integrated intensity in the Q_1 manifold (relative to the total spectrum as in Figure 1). The linear relationship reflects the consistency of the overall analysis.

The rate constant for intersystem crossing among the dyads and monomers in toluene and benzonitrile falls into a narrow range of 16–23 ns⁻¹ because solvent polarity does not significantly affect the spin–orbit coupling that underlies the $S_1 \rightarrow T_1$ process. The results show that neither does change in electron distributions and other electronic characteristics resulting from dyad formation.

The rate constants for internal conversion can be summarized as follows: (1) k_{ic} is greater for bacteriochlorin versus chlorin monomers, as expected based on the lower S_1 energy and the energy-gap law.⁵⁴ (2) k_{ic} for the chlorin and bacteriochlorin benchmarks are not sensitive to the solvent polarity, as expected based on the first point and the fact that the position of the lowest-energy absorption band, reflecting the S_1 energy, is similar in toluene and benzonitrile. (3) k_{ic} for the chlorin dyads is on the average 2-fold larger in benzonitrile versus toluene. (4) k_{ic} for the bacteriochlorin dyads is on the average larger by roughly an order of magnitude in benzonitrile versus toluene. The latter point

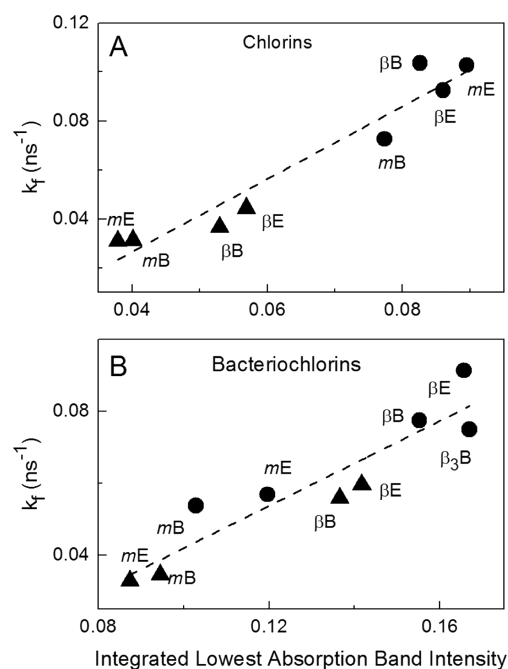


Figure 2. Rate constant k_f (in units of ns⁻¹) versus the integrated oscillator strengths of the lowest absorption bands in hydroporphyrin dyads (circles) and benchmarks (triangles). Each point is identified by the linker site and linker, with the full name given in Table 1.

reflects the greatly enhanced yield of internal conversion described above and is analyzed in more detail in the Discussion Section.

3.6. Redox Properties. The redox potentials for the chlorins and bacteriochlorins are listed in Table 4. The potentials for the

Table 4. Redox Properties of Compounds^a

cmpd	E_{ox1} (V)	E_{red1} (V)
C- β B	+0.61	-1.45
C_2 - β B	+0.58 ^b	-1.38, -1.45
C- β E	+0.55	-1.53
C_2 - β E	+0.61, +0.51	-1.44, -1.55
C-mB	+0.66	-1.41
C_2 -mB	+0.62 ^b	-1.37 ^b
BC- β B	+0.29	-1.38
BC_2 - β B	+0.38, +0.29	-1.29, -1.36
BC- β E	+0.29	-1.36
BC_2 - β E	+0.38, +0.26	-1.29, -1.41
BC-mB	+0.26	-1.48
BC_2 -mB	+0.34, +0.25	-1.35, -1.46

^aAll potentials (measured in V) were measured on compounds in butyronitrile containing 0.1 M tetrabutylammonium hexafluorophosphate. The potentials are adjusted so that the ferrocene couple has a value of 0.190 V under the conditions of the measurement. ^bWaves broader than those of the monomers.

first oxidation (E_{ox1}) and the first reduction (E_{red1}) for the benchmarks are generally consistent with those reported for other monomeric chlorins and bacteriochlorins.⁵⁵ Compared to the benchmarks, the chlorin dyads are both slightly easier to oxidize (by 0.03–0.04 V) and reduce (by 0.04–0.09 V). The bacteriochlorin dyads are also slightly easier to oxidize (by up to 0.03 V) and in some cases easier to reduce (by 0.02–0.07 V).

The most distinct difference in the redox characteristics of the dyads versus monomers is that the former (in most cases) exhibit doubled redox waves. In particular, the first reduction wave for all the dyads except $C_2\text{-mB}$ exhibits two resolved or partially resolved features at the potentials listed in Table 4. The reduction wave for $C_2\text{-mB}$ is broader than that of the monomers, suggesting two underlying features. Similarly, the first oxidation wave for all the dyads except $C_2\text{-mB}$ and $C_2\text{-}\beta\text{B}$ is split into two features. The oxidation waves for $C_2\text{-mB}$ and $C_2\text{-}\beta\text{B}$ are also broader than those of the monomers, again suggesting two underlying features. The observation of split redox waves in the dyads is direct evidence for strong linker-mediated electronic coupling between the two constituent hydroporphyrins in the ground electronic state.

3.7. MO Characteristics. DFT calculations were performed on the dyads and the benchmarks, starting with the optimized molecular geometry. The β -linked dyads $\text{BC}_2\text{-}\beta\text{E}$ (Figure 3A

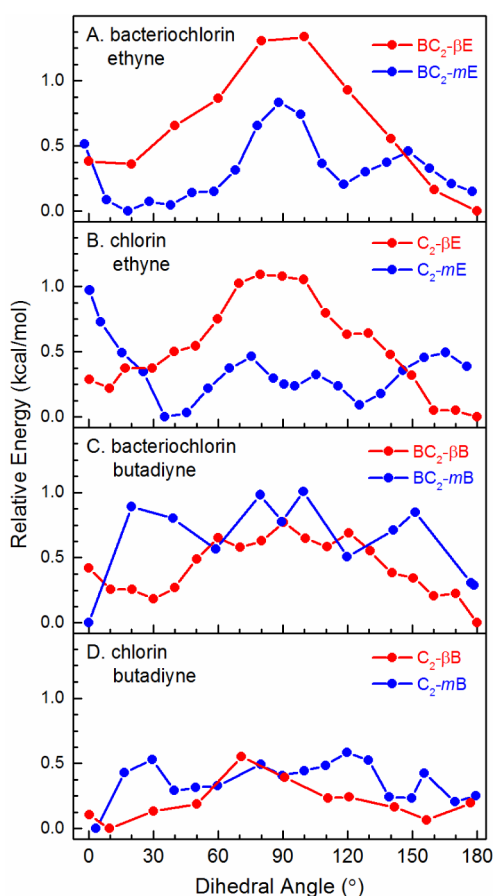


Figure 3. Relative total energy versus dihedral angle for hydroporphyrin dyads.

red), $C_2\text{-}\beta\text{E}$ (Figure 3B, red), and $\text{BC}_2\text{-}\beta\text{E}$ have a minimum-energy structure with the bacteriochlorin macrocycles coplanar in a *trans*-conformation (Chart 1), for which the torsional angle is defined as 180° . Accessing different torsional angles involves rotation about the linker axis. For dyads $\text{BC}_2\text{-mE}$ (Figure 3A, blue) and $C_2\text{-mE}$ (Figure 3B, blue), the minimum-energy structure has noncoplanar macrocycles with torsional angles of $\sim 19^\circ$ and $\sim 39^\circ$, which are closer to the *cis*-coplanar conformation, for which the torsional angle is defined as 0° . Regardless of the torsional angle for the minimum-energy structure, the barriers to internal rotation for all four dyads

containing an ethynyl linker are quite low (<1.5 kcal/mol), consistent with previous calculations^{37,38} on the same or similar dyads.

The barriers to internal rotation are smaller for the bacteriochlorin dyads (≤ 1 kcal/mol; Figure 3C) and chlorin dyads (≤ 0.5 kcal/mol; Figure 3D) that employ the butadiyne linker. The bacteriochlorin dyads have a minimum-energy structure at $\sim 180^\circ$ (*trans*-coplanar) for $\text{BC}_2\text{-}\beta\text{B}$ and at $\sim 0^\circ$ (*cis*-coplanar) for $\text{BC}_2\text{-mB}$. Both chlorin analogues $C_2\text{-}\beta\text{B}$ ($\sim 10^\circ$) and $C_2\text{-mB}$ ($\sim 3^\circ$) have minimum-energy structures close to the *cis*-coplanar conformation. In general, the calculations of the minimum energy for the butadiyne-linked hydroporphyrin dyads do not converge readily, because there is little gradient toward the minimum. Thus, in these cases there is uncertainty in the global and local minima, compounding the low barriers that allow the dyad to sample essentially the full space of internal rotational conformations at room temperature.

Figures 4–7 present the electron-density distributions and energies of the frontier MOs for the four sets of dyads and benchmarks (chlorins or bacteriochlorins with β - or *meso*-linkages). Analysis of these diagrams is aided by reference to Figure 8, which illustrates (1) abbreviations for the frontier MOs of benchmark monomers [HOMO–1 (H^{-1}), HOMO (H), LUMO (L), LUMO+1 ($L+1$)], (2) that the frontier MOs of a dyad are linear combinations of monomer MOs due to strong linker-mediated interactions,^{56,57} denoted with superscript “1” (lower energy) and “h” (higher energy) on the appropriate monomer orbital (e.g., L^1 and L^h for the dyad MOs originating from the LUMO of the two monomers), and (3) that the ordering of the eight dyad MOs may differ depending on the magnitude of the “splitting” within pairs of dyad MOs relative to the spacing between the monomer MOs.

The splitting within a given dyad MO pair depends on the extent of linker-mediated interaction between constituent macrocycles. These interactions depend on the linker (ethyne versus butadiyne) and the electron density of the monomer orbital at the macrocycle attachment site (β -pyrrole or *meso*-carbon). Typically the HOMO of chlorins is an $a_{1u}(\pi)$ -like orbital (D_{4h} symmetry designation), which places considerably more electron density at the β -pyrrole sites than at the *meso*-carbons, while the HOMO–1 is an $a_{2u}(\pi)$ -like orbital, which has the reverse relative electron densities at the two positions. This is the case for $C\text{-}\beta\text{B}$, $C\text{-mB}$, and $C\text{-}\beta\text{E}$. However, for $C\text{-mE}$ there is a reversal of monomer MOs such that the HOMO is $a_{2u}(\pi)$ -like and HOMO–1 is $a_{1u}(\pi)$ -like. Such a reversal does not occur for $\text{BC}\text{-mE}$, which like $\text{BC}\text{-mB}$, $\text{BC}\text{-}\beta\text{E}$, and $\text{BC}\text{-}\beta\text{B}$ has the normal hydroporphyrin $a_{1u}(\pi)$ -like HOMO and $a_{2u}(\pi)$ -like HOMO–1 because of the much larger energy spacing between these orbitals in the unsubstituted bacteriochlorin versus chlorin monomer (due to hydrogenation of a second pyrrole ring in the former).

With this foundation in hand, the following key points are gleaned from Figures 4–7:

(1) The β -linked dyads ($C_2\text{-}\beta\text{B}$, $C_2\text{-}\beta\text{E}$, $\text{BC}_2\text{-}\beta\text{B}$, $\text{BC}_2\text{-}\beta\text{E}$) have the simple MO ordering as follows: HOMO–3/HOMO–2 (H^{-1}/H^{-1^h}), HOMO–1/HOMO (H^1/H^h), LUMO/LUMO + 1 (L^1/L^h), and LUMO+2/LUMO+3 ($L+1^1/L+1^h$). H^h and L^1 of each of these dyads have significant MO density on the linkers while H^1 and L^h do not, resulting in a significant splitting between the pairs H^1/H^h and L^1/L^h , as illustrated schematically in Figure 8A. Neither of the members within the H^{-1}/H^{-1^h} and $L+1^1/L+1^h$ pairs has appreciable density on the linker, and thus they have essentially the same energy (and do not show the splitting illustrated in Figure 8A).

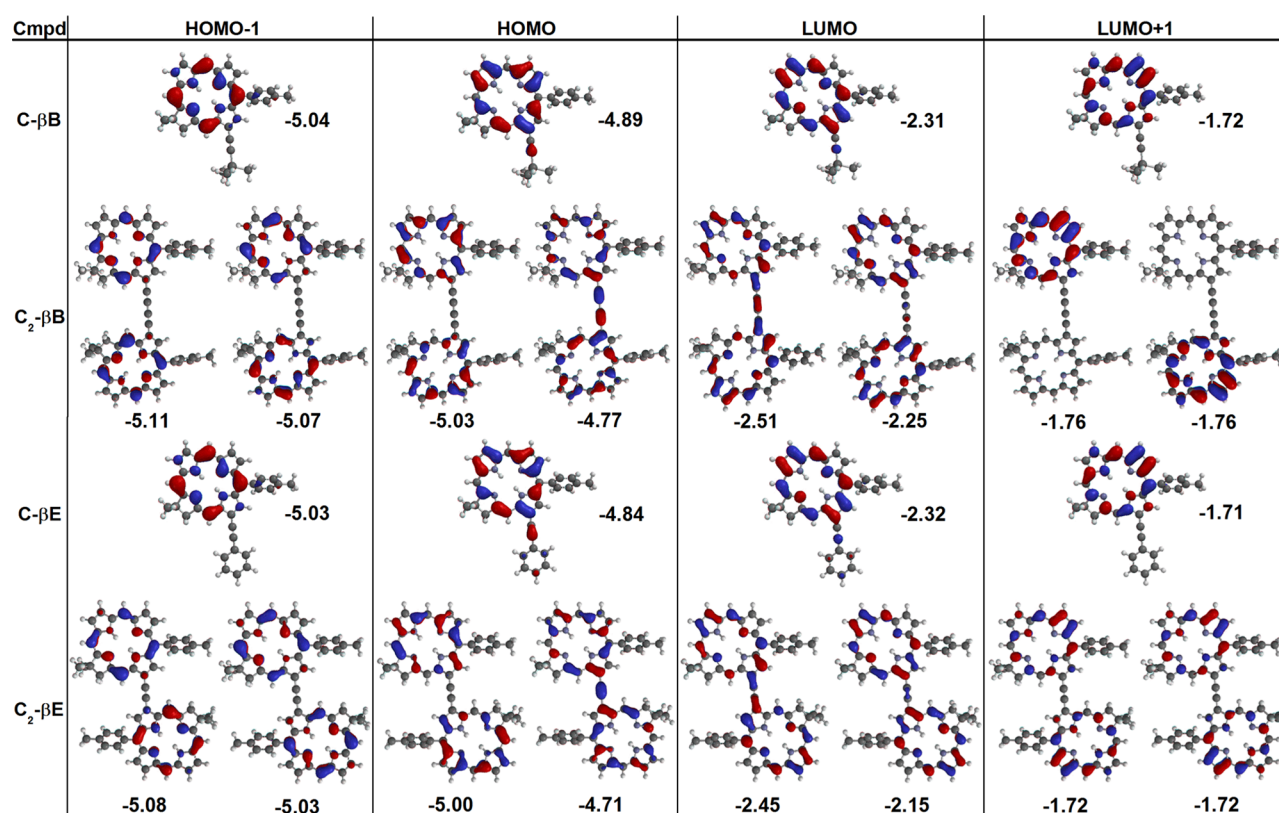


Figure 4. Frontier MOs and MO energy levels of the β -linked chlorin benchmarks and dyads.

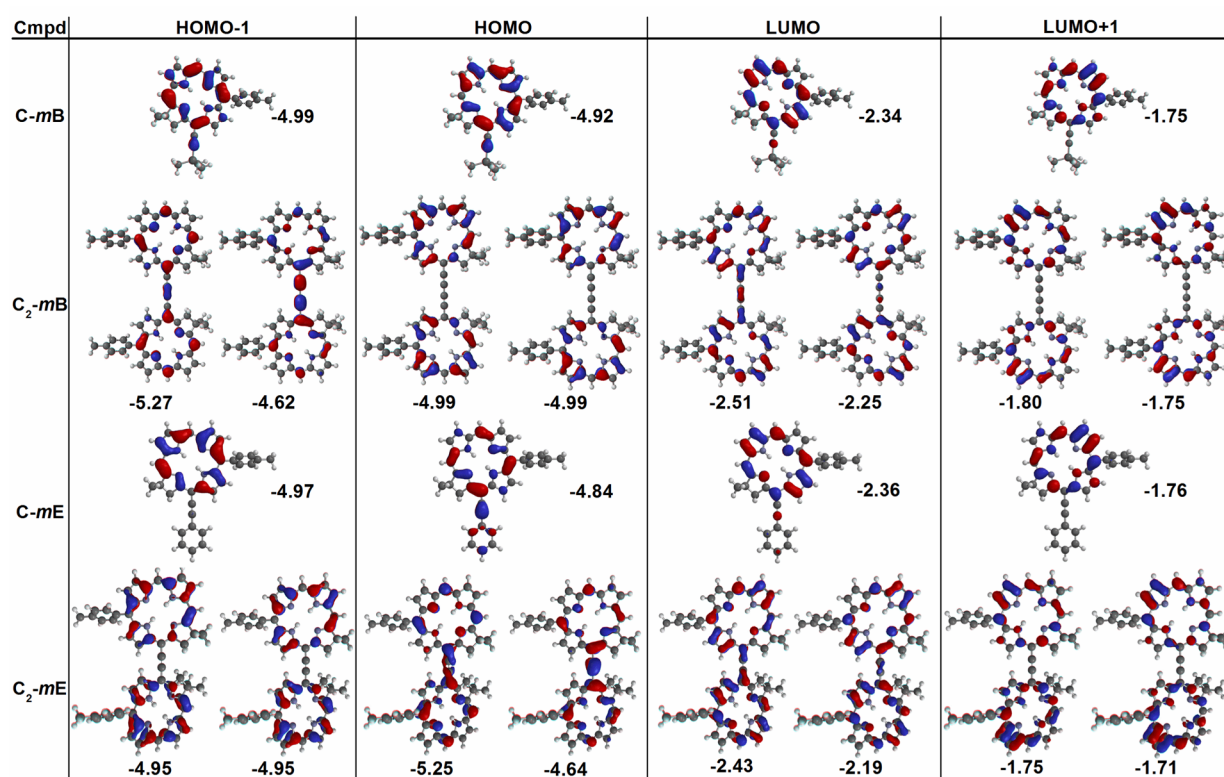


Figure 5. Frontier MOs and MO energy levels of the *meso*-linked chlorin benchmarks and dyads.

(2) Compared to the β -linked dyads, the effects of macrocycle interactions on the MO characteristics are more varied among the *meso*-linked dyads. For the unoccupied MOs, $L+1^h$ and $L+1^h$

are almost degenerate for C₂-*m*B (−1.80 and −1.75 eV) and C₂-*m*E (−1.75 and −1.71 eV), reflecting the lack of significant MO density on the linker (Figure 5). The splitting is 2–3-fold larger

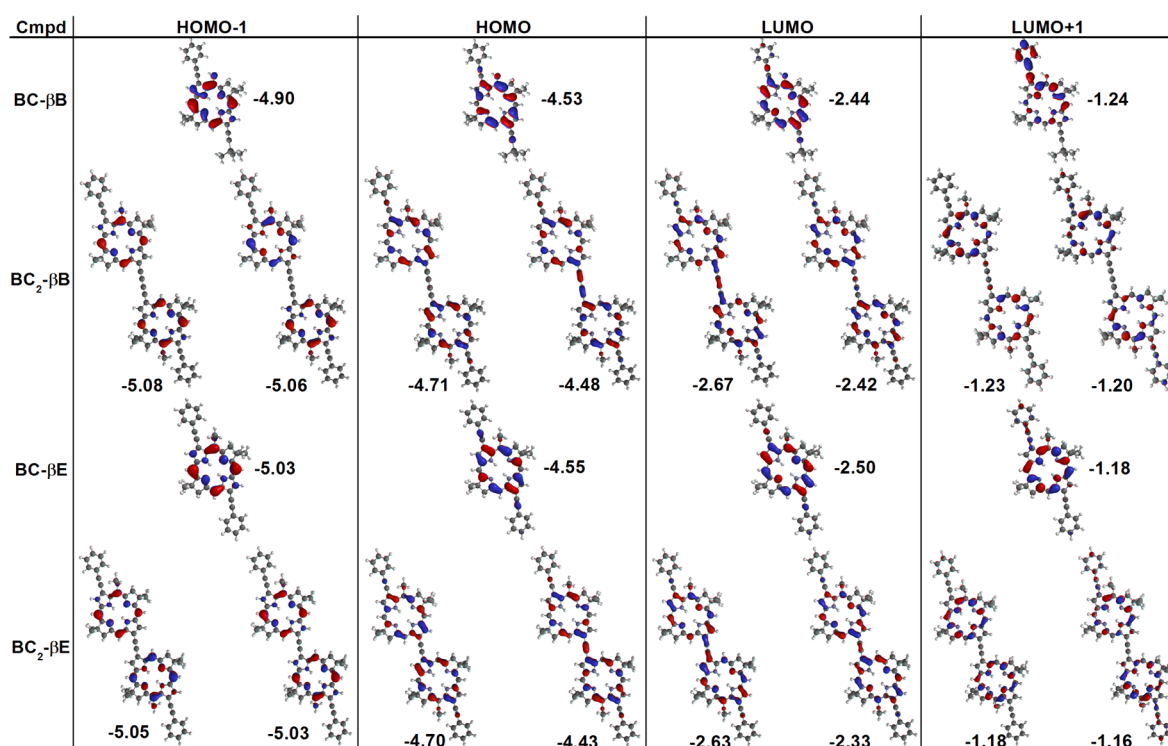


Figure 6. Frontier MOs and MO energy levels of the β -linked bacteriochlorin benchmarks and dyads.

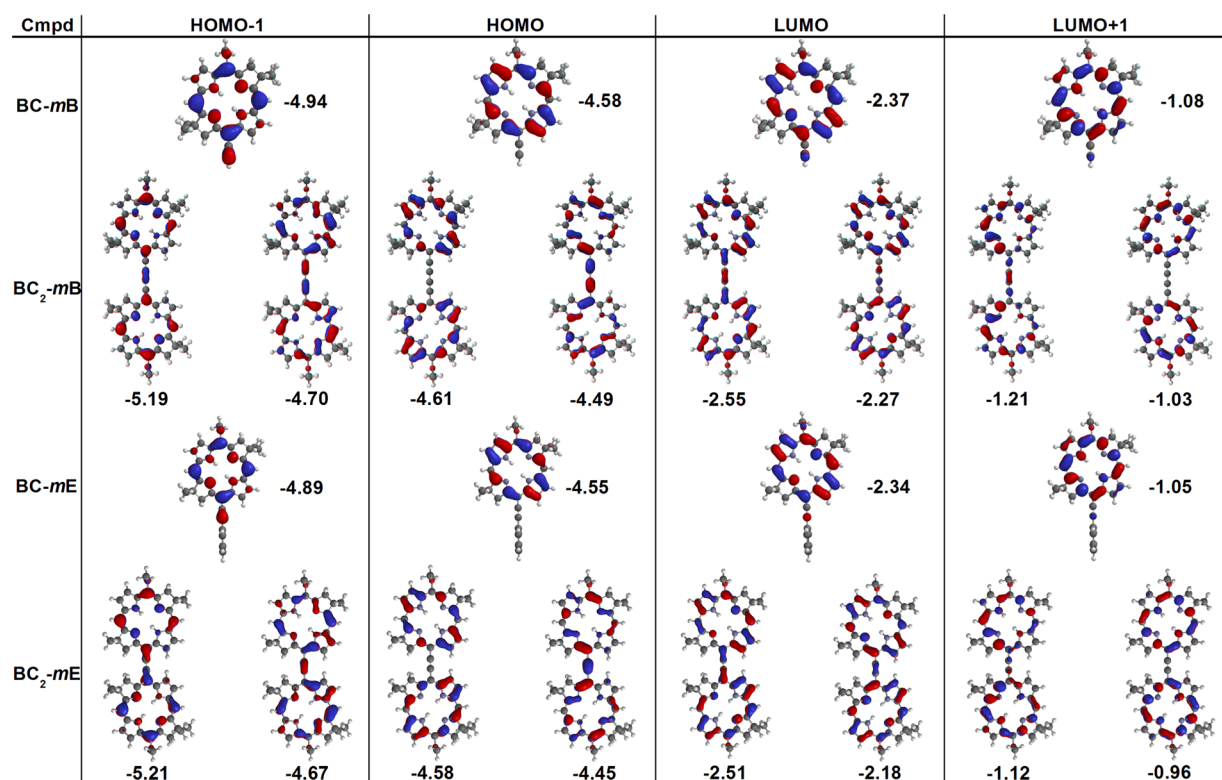


Figure 7. Frontier MOs and energies of *meso*-linked bacteriochlorin benchmarks and dyads.

for $L+1^l$ and $L+1^h$ of the bacteriochlorin analogues **BC₂-*m*B** (-1.21 and -1.03 eV) and **BC₂-*m*E** (-1.12 and -0.96 eV) (Figure 7). Even substantially larger splitting is observed between L^l and L^h of **C₂-*m*B** (-2.51 and -2.25 eV) and **C₂-*m*E** (-2.43 and -2.19 eV), and of **BC₂-*m*B** (-2.55 and -2.27 eV) and **BC₂-*m*E** (-2.51 and -2.18 eV).

(3) The energy ordering among the occupied MOs shows the most substantial variations among the *meso*-linked dyads. This behavior derives from the above-noted characteristics of the filled orbitals [$a_{2u}(\pi)$ - and $a_{1u}(\pi)$ -like] and the reversal for benchmark **C-*m*E** versus the other cases. Because of the large electron density at the *meso*-positions for the $a_{2u}(\pi)$ -like orbital, the MOs

formed from this type of orbital for C_2 - mE are the pair HOMO (H^h , -4.64 eV) and HOMO-3 (H^l , -5.25 eV) and for C_2 - mB are the pair HOMO ($H-1^h$, -4.62 eV) and HOMO-3 ($H-1^l$, -5.27 eV) (Figure 5). In each case the large dyad MO splitting (0.61 and 0.65 eV) reflects the strong linker-mediated intermacrocycle electronic coupling. The split $a_{2u}(\pi)$ -derived pair of orbitals sandwich the a_{1u} -derived dyad HOMO-1 and HOMO-2 (as illustrated in Figure 8B for the case where the monomer HOMO is a_{2u} -like), which are degenerate for both C_2 - mE (-4.95 eV) and C_2 - mB (-4.99 eV), reflecting the lower electron density at the linker site in the monomer and on the linker in the dyad. In contrast to the *meso*-linked chlorins, for the bacteriochlorin analogues BC_2 - mB and BC_2 - mE (Figure 7) the HOMO/HOMO-1 [$(-4.49$ eV)/ $(-4.61$ eV) and $(-4.45$ eV)/ $(-4.58$ eV)] are derived from the $a_{1u}(\pi)$ -like monomer HOMO (-4.58 and -4.55 eV) and the HOMO-2/HOMO-3 [$(-4.70$ eV)/ $(-5.19$ eV) and $(-4.67$ eV)/ $(-5.21$ eV)] are obtained from the monomer HOMO-1 (-4.94 and -4.89) due to the large splitting between the bacteriochlorin monomer MOs.

4. DISCUSSION

The sets of chlorin and bacteriochlorin dyads studied herein exhibit optical, redox, excited-state, and MO characteristics that differ from each other and the corresponding benchmarks due to strong electronic interactions between the constituent macrocycles. Many of these characteristics make such dyads useful as light-harvesting elements in solar-conversion systems or as optical imaging agents. In particular, the dyads exhibit (1) significant bathochromic shifts of the lowest-energy absorption band (deeper) into the NIR region, (2) significant optical splitting that affords effectively broader spectral coverage, (3) significant fluorescence yields (Φ_f) that are enhanced relative to the benchmarks in most cases, more substantially for the chlorin dyads, (4) retention of relatively long excited-state lifetime (τ_s) except for the bacteriochlorin dyads in benzonitrile, (5) oxidation and reduction potentials that are generally comparable to the benchmarks, albeit with split redox waves, and (6) a reduced yield of intersystem crossing. One unfavorable characteristic of the dyads versus the monomers is that the bacteriochlorin dyads exhibit excited-state quenching in benzonitrile. This observation is also of interest because the dyads are symmetrical with strongly coupled subunits. Such dyads do not possess actual states with net charge transfer (CT) character that are stabilized in a polar medium and thereby provide an additional decay pathway for an S_1 state, which is the common explanation for such quenching in asymmetric and more weakly coupled arrays (*vide infra*). Collectively, the availability in the present study of such a diverse set of observations on sets of related dyads allows for a unified analysis in terms of strong interchromophore electronic interactions.

Typically, the observation of shifted and/or split absorption features for a dyad or larger molecular array is placed in the context of an exciton model. This model is based on the coupling of excited-state transition dipoles and assumes no significant ground-state interactions.^{54,58} The observation that the redox potentials of the hydroporphyrin dyads are split (Table 4), evidence for strong ground electronic state interactions, indicates that the exciton-coupling model is not an appropriate descriptor for these architectures. This view is further supported by the MO characteristics of the dyads, which reveal pairwise linear combinations of monomer MOs, with electron density generally delocalized over the entire molecule (Figures 4–7), consistent

with previous theoretical predictions for tetrapyrrolic dyads bearing conjugating linkers.³⁸

Furthermore, in a simple exciton model involving coupling of excited-state transition dipoles, the magnitude of the splitting of the absorption bands is proportional to the square of the strength of the monomer transition. In such a model, the perturbations to the Q_y bands of the bacteriochlorins generally would be much greater than those for the chlorins, due to the greater oscillator strength of the Q_y transition of constituent bacteriochlorins versus chlorins. However, the bathochromic shifts and splitting of the Q_y bands of some of the chlorin dyads are comparable to those of the bacteriochlorin analogues (Table 2). Along the same lines, in a simple exciton model there would be relatively small effects of interchromophore electronic interactions on the weak Q_x features of the dyad versus the monomers. However, as noted in the Results section, the Q_x bands of *meso*-linked hydroporphyrin dyads show a shift of up to ~ 2000 cm^{-1} and a splitting up to ~ 1000 cm^{-1} . Such values are comparable to or even larger than those for the Q_y (and Soret) features. Collectively, such effects for all the absorption bands cannot be understood within the framework of a simple exciton model. Alternatively, as described above and further below, such observations can be qualitatively understood in terms of the effects of strong electronic interactions on the MOs of the dyad versus monomers. This includes the differences observed in the different spectral regions (Soret, Q_x , and Q_y) depending on the site of linker attachment and on which orbitals are most affected by the linker-mediated electronic interactions.

One characteristic of the dyads that requires additional comment concerns the nature of the torsional potential energy surface for rotation about the linker. The DFT calculations reported here and previously^{37,38} indicate that the barriers to internal rotation are relatively small (< 1.5 kcal/mol), often with a maximum in the vicinity of 90° (Figure 3). The calculations further reveal that the potential well is relatively broad in the vicinity of the global and local minima. The pairwise mixing and splitting of the dyad MOs depend on the exact value of the torsional angle; such splitting vanishes at 90° , where electronic communication *via* the linker is absent. Accordingly, a rigorous model for the effects of torsional motion on the electronic properties of the dyads would require inclusion of the full vibrational manifold for the low-frequency, anharmonic torsional motion on both the ground and excited electronic state potential surfaces. Such a treatment is beyond the scope of the present effort. In this connection, it should be noted that the low-barrier nature of the torsional potential surface renders the concept of distinct internal-rotation “conformers” an inappropriate descriptor of the dyads. The “conformational space” accessed by the dyad at a given temperature reflects the Boltzmann populations of all the thermally accessible sublevels of all the various torsional (and macrocycle) modes and the associated types and amplitudes of molecular motions. Therefore, we have used a static description of the effects of strong electronic coupling. Although this description is not rigorously correct, it provides a qualitatively useful view of the system and is consistent with the finding that the MOs of the dyads are best represented by pairwise linear combinations of monomer MOs.

The optical spectra of tetrapyrroles are often described in terms of Gouterman’s four-orbital model.^{3,51,52} The basis of this model is that the NUV to NIR optical spectra, and in particular the relative wavelengths and intensities of the B_y , B_x , Q_x , and Q_y bands, can be understood to a first approximation in terms of electron promotions involving four frontier MOs, the $H-1$, H , L ,

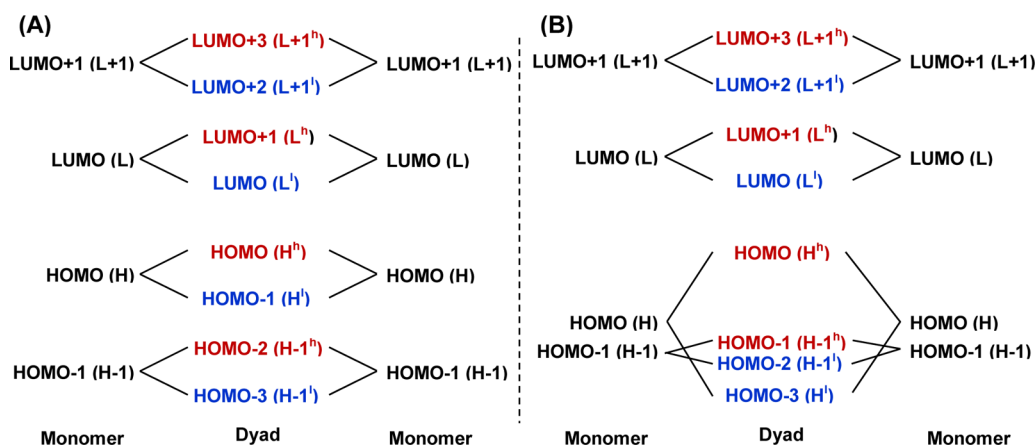


Figure 8. Nomenclature for the frontier MOs of a hydroporphyrin monomer and the linear combinations that are the frontier MOs of a dyad. Panel (A) illustrates the simplest case of equal splitting of each pair of dyad MOs, with splitting smaller than the spacing between monomer MOs. Panel (B) shows a more complex case of large splitting of dyad MOs arising from monomer HOMO and small spacing of the monomer HOMO and HOMO-1.

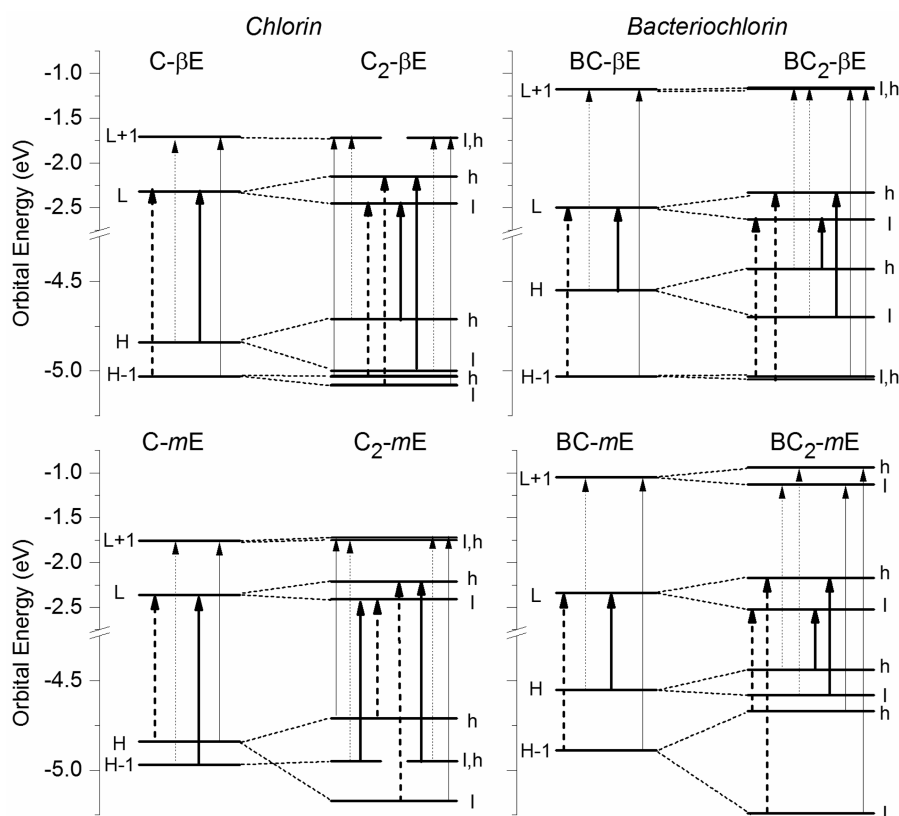


Figure 9. Representative allowed one-electron promotions of the hydroporphyrin dyads assuming coplanar macrocycles in a C_{2h} symmetry) as in Chart 1. For the monomers, the solid and dashed arrows indicate the y - and x -axis promotions, respectively. The promotions in the dyads were deduced from the symmetries of the linear combinations of the monomer orbitals.

and L+1. The B_y , B_x , Q_y , and Q_x excited states are derived from binary combinations (constructive or destructive) of the four one-electron excited-state configurations. Direct application of this model to understand the wavelengths and intensities of the optical spectra of the strongly coupled hydroporphyrin dyads is clearly an oversimplification. However, inspection of Figure 1 indicates that the spectra of the dyads have features in the same general spectral regions as the benchmarks, albeit shifted and split in many instances. Thus, in analyzing the optical characteristics of the dyads, it is convenient to use a general framework that provides a link to that used for the monomers. In

particular, key aspects of the spectra of the dyads are associated with one-electron promotions between the dyad MOs, which are formed by the same four frontier monomer MOs that are the basis of the four-orbital model. The MO diagrams given in Figures 4–7 suggest that this is a reasonable approach. Furthermore, analysis of the signs of the dyad MOs indicates that 8 of the 16 possible one-electron promotions between the 8 dyad orbitals are optically allowed if the two macrocycles of the dyad are in the coplanar $trans$ -configuration (C_{2h} symmetry, as in Chart 1). These promotions are shown in Figure 9.

The illustration shows four pairs of one-electron promotions. The energy splitting within each pair derives from the combination of split-filled dyad orbitals (e.g., H^l and H^h) and split-empty dyad orbitals (e.g., L^l and L^h) relative to those of the monomer (e.g., H and L). The energy splitting within each pair of one-electron promotions for the dyad leads to split levels in the excited-state manifold and to split optical absorption bands (e.g., $Q_{1\beta}$ and $Q_{1\alpha}$). It should be noted that all 16 of the one-electron promotions (8 are shown in Figure 9) are allowed if a dyad assumes the coplanar *cis*-configuration. Dyads that have a minimum in the torsional potential at an intermediate angle will have all the transitions allowed to some degree (e.g., those with *meso*-ethyne linkages). Additionally, even if the minimum is at or near 180° (coplanar *trans*-configuration), the barriers to internal rotation to access other regions of the torsional potential are very low (Figure 3). The consequence will be a broadening or doubling of the bands in the absorption spectra depending on the extent to which the dyads access internal torsional angles away from 180° . Such may underlie the general observation that some *meso*-linked dyads exhibit spectra with more or broader features than the β -linked analogues (Figure 1).

For dyads that assume a *trans*-coplanar configuration (e.g., β -linked dyads $C_2\text{-}\beta E$, $BC_2\text{-}\beta B$, and $BC_2\text{-}\beta E$), the symmetry-allowed one-electron promotions/configurations for which the analogues in monomers would pairwise mix to give the B_y and Q_y states/bands are $[H^h \rightarrow L^l]$, $[H^l \rightarrow L^h]$, $[H-1^h \rightarrow L+1^l]$, and $[H-1^l \rightarrow L+1^h]$. Following the logic that for a bacteriochlorin monomer the lowest-energy absorption band (Q_y) is composed primarily of $[H \rightarrow L]$, with a lesser contribution from $[H-1 \rightarrow L+1]$,^{10,59,60} the split $Q_{1\beta}$ and $Q_{1\alpha}$ bands (Figure 1) of the dyad would derive primarily from the splitting between the $[H^h \rightarrow L^l]$ and $[H^l \rightarrow L^h]$ one-electron promotions. Similarly, splitting in the visible region for the dyad ($Q_{2\beta}$ and $Q_{2\alpha}$) would derive from the split energy levels derived from the $[H-1^h \rightarrow L^l]$, $[H-1^l \rightarrow L^h]$, $[H^h \rightarrow L+1^l]$, and $[H^l \rightarrow L+1^h]$ one-electron promotions, for which the analogues on the monomer give rise to the Q_x (and B_x) bands.

The large contribution of $[H \rightarrow L]$ in the lowest-energy absorption band of bacteriochlorin monomers is directly manifested in the spectral characteristics of the bacteriochlorin dyads. In particular, the splitting of the one-electron promotions and splitting of the lowest absorption bands have a clear linear relationship (Figure 10, red circles). Unlike the bacteriochlorin dyads, the chlorin analogues do not show such a clear

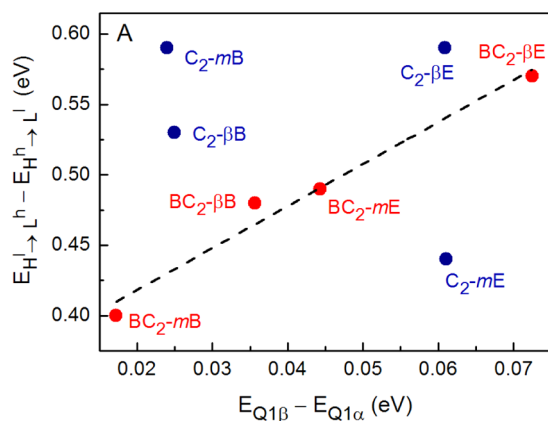


Figure 10. $E_{H^l \rightarrow L^h} - E_{H^h \rightarrow L^l}$ vs lowest absorption band splittings for the hydrophorphyrin dyads. The line is a guide to the eye.

relationship (blue circles). This finding likely arises from several sources. One is that there is a greater contribution of the dyad configurations analogous to the monomer $[H-1 \rightarrow L+1]$ along with $[H \rightarrow L]$ to the lowest-energy excited-state manifold and absorption contour.^{3,8} Additionally, for certain *meso*-linked chlorin dyads (e.g., $C_2\text{-}mE$), the change in orbital ordering (e.g., $a_{2u}(\pi)$ -like versus $a_{1u}(\pi)$ -like orbitals) results in a change in polarizations. Moreover, as noted above, for these dyads and others that access torsional angles away from 180° , which defines the *trans*-coplanar configuration of macrocycles, the 8 one-electron promotions not shown in Figure 1 become allowed to varying degrees, giving rise to additional (or broader) features in the absorption spectra. The associated range of twisted molecular geometries also result in a distribution of electronic couplings that are smaller than those for the *trans*-coplanar configuration. Regardless, all of these characteristics are a manifestation of the strong linker-mediated intermacrocycle electronic interactions in the dyads and how the interactions are altered by detailed architectural characteristics.

The last major topic is the related effects of strong electronic coupling on the decay properties of the lowest singlet excited state (S_1). The S_1 state of all hydrophorphyrin dyads and benchmark monomers decay by $S_1 \rightarrow S_0$ fluorescence, $S_1 \rightarrow T_1$ intersystem crossing, and $S_1 \rightarrow S_0$ internal conversion with rate constants k_f , k_{isc} , and k_{ic} , respectively. The values derived above are given as the corresponding time constants (in nanoseconds) in Tables 2 (chlorins) and 3 (bacteriochlorins). In general, the dyads exhibit larger k_f and k_{ic} compared to the monomers, as well as less systematic variation in k_{isc} . The larger k_{ic} follows from the energy gap law;⁵⁴ the S_0 - S_1 energy gaps of the dyads are consistently lower than those of the benchmarks. Torsional rotations involving the conjugated linker may play an additional role in accelerating the internal conversion process. The larger k_f for $S_1 \rightarrow S_0$ fluorescence for the dyads are paralleled by larger intensities for $S_0 \rightarrow S_1$ absorption for the dyads versus monomers, consistent with the relationship of the Einstein coefficients.⁵⁴

A notable observation on the S_1 characteristics of the dyads is the large solvent polarity dependence of k_{ic} for the bacteriochlorins, which leads to minimal fluorescence of these dyads (but not monomers) in benzonitrile. Such quenching is common for asymmetric systems such as tetrapyrrole-based donor-acceptor architectures^{5,6} and aryethyne-linked chlorin-bacteriochlorin dyads,³⁵ and also has been observed for symmetric strongly coupled vinyl-linked chlorophyllide dyads related to those studied here.^{61,62} To understand the origin of such quenching, we use a framework that has been employed for porphyrin sandwich complexes^{56,57} and the native bacteriochlorophyll dimer and mutant bacteriochlorophyll-bacteriopheophytin dimer in photosynthetic reaction centers.⁶³⁻⁶⁶ Although these two systems differ structurally from each other and the dyads under study herein (including the absence of covalent linkage for the reaction-center dimer), all of the systems share substantial orbital overlap and, thus, strong electronic interactions between constituents.

For typical asymmetric dyads with subunits A and B (and relatively weak A-B electronic coupling), the states of the system from higher to lower energy could be exemplified as $A^-B^+ > A^+B^- > B^* > A^*$, where A^* is the normal S_1 excited state of chromophore A, lower than B^* , and A is easier to oxidize and harder to reduce than B. A substantial reduction in τ_s and Φ_f for A^* for the dyad in a polar versus nonpolar medium would normally imply that solvent stabilization has dropped CT state

A^+B^- (and perhaps also A^-B^+) below, or thermally accessible above, A^* such that the process $A^* \rightarrow A^+B^- \rightarrow$ ground state provides an additional excited-state deactivation route.

For symmetrical (and strongly coupled) dyads such as those studied here, the analogous set (A^-A^+ , A^+A^- , A^*A , and AA^*) do not exist as observable states but form the zeroth-order basis set of the system. In the absence of perturbations such as transient solvent symmetry breaking, the two CT configurations A^-A^+ and A^+A^- have equal energies, and linear combinations give charge resonance (CR) configurations ($A^+A^- \pm A^-A^+$). Similarly, the two locally excited configurations A^*A and AA^* have equal energies, and admixtures produce “exciton” configurations ($A^*A \pm AA^*$). These four configurations give the first-order basis set in this framework. Typically, the S_1 excited state of such a dyad in nonpolar media will be dominated by either ($A^*A + AA^*$) or ($A^*A - AA^*$), whichever is lower in energy, depending on the dyad architecture (e.g., face-to-face or end-to-end), with little admixture of a ($A^+A^- \pm A^-A^+$) CR configuration because they lie at a much higher energy. In a polar medium, ($A^+A^- \pm A^-A^+$) will be stabilized and whichever is lowest will mix more substantially with the lowest of ($A^*A \pm AA^*$) to *redefine* the S_1 state. If the solvent stabilization is significant enough so that the lowest of ($A^+A^- \pm A^-A^+$) drops energetically below the lowest of ($A^*A \pm AA^*$), the new lowest excited state of the dyad will have primarily CR character but still no net CT character.

Thus, for symmetric strongly coupled dyads, polar solvent stabilization does much more than simply lower a “CT state” to near or below a nominally unchanged S_1 state, providing a new S_1 decay route that underlies excited-state quenching in asymmetric weakly coupled cases. It is the altered nature of the set of dyad states in the polar versus nonpolar medium (not simply a change in relative energies of states with basically fixed character) that underlies the photophysics of symmetric strongly coupled dyads. There may be several contributions to the observed behavior. The increased configurational mixing into the S_1 state of configurations that have little radiative probability (CR configurations) enhances deactivation in polar versus nonpolar medium. The CR contribution may enhance decay due to coordinate displacements of the excited- versus ground-state potential energy surfaces. In addition, motions that alter the spatial relationship of the two macrocycles of the dyad may enhance nonradiative decay to S_0 by modulating the energies of the CR configurations (*via* Coulomb interactions), the extent of mixing with the exciton configurations, and thus the nature of the S_1 state.

The greater quenching of bacteriochlorin versus chlorin dyads with an increase in solvent polarity derives from the relative energies of the CR configurations. Bacteriochlorins are considerably easier to oxidize than chlorins, whereas the reductions of the two types of hydrophorphyrins occur at more similar potentials.⁵⁵ For example, examination of Table 4 shows that the average (monomer and dimer) potential for the first oxidation is +0.59 V for chlorins and +0.30 V for bacteriochlorins, a difference of 0.29 V. The average potential for the first reduction is -1.44 V for chlorins and -1.38 V for bacteriochlorins, a difference of 0.06 V. Subtraction of the average reduction from oxidation values gives 2.03 V for chlorins and 1.67 V for bacteriochlorins, a difference of 0.36 eV. In comparison, the average (e.g., monomer Q_y and dyad $Q_{1\beta}$ and Q_{1a}) S_1 energy from Table 1 is 1.86 eV for chlorins and 1.62 eV for bacteriochlorins, a difference of 0.24 eV.

These comparisons show that the energies of the CR configurations ($A^+A^- \pm A^-A^+$) of the bacteriochlorin dyads

will be lower than those of the chlorin dyads and closer to the ($A^*A \pm AA^*$) configurations that principally define the S_1 state. As a result, there will be increased quantum mechanical (not simply thermal) mixing and an increased percent contribution of one of the ($A^+A^- \pm A^-A^+$) configurations along with one of the ($A^*A \pm AA^*$) configurations to the S_1 state. Collectively, such effects can account for the large solvent-polarity dependence of k_{ic} in the bacteriochlorin dyads.

5. CONCLUSIONS

The hydrophorphyrin dyads examined herein have significantly modified spectral, redox, molecular-orbital, and photophysical characteristics relative to the benchmark monomers. These properties are a manifestation of the strong electronic coupling between the constituent hydrophorphyrins in the dyads that is mediated by the ethynyl or butadiynyl linker. These physicochemical properties of the synthetic hydrophorphyrin dyads may prove useful in light-harvesting arrays for solar-energy conversion and fluorescent probes for NIR imaging.

■ ASSOCIATED CONTENT

Supporting Information

The Supporting Information is available free of charge on the ACS Publications website at DOI: 10.1021/acs.jpca.5b10686.

Synthesis methods and chemical characterization data; tabulated spectral characteristics of the dyads and benchmarks in benzonitrile; absorption and fluorescence spectra of dyads and benchmarks in benzonitrile; MO characteristics of $BC_2\text{-}\beta_3B$ and resolution-enhanced absorption spectra of compounds in toluene; complete refs 8, 11, 12, 25, and 40 (PDF)

■ AUTHOR INFORMATION

Corresponding Authors

*E-mail: rbirge@uconn.edu (R.R.B.).

*E-mail: mptaszek@umbc.edu (M.P.).

*E-mail: holten@wustl.edu (D.H.).

*E-mail: david.bocian@ucr.edu (D.F.B.).

Notes

The authors declare no competing financial interest.

■ ACKNOWLEDGMENTS

Work at WU and UCR was supported by grants from the Division of Chemical Sciences, Geosciences, and Biosciences, Office of Basic Energy Sciences of the U.S. Department of Energy, to D.F.B. (DE-FG02-05ER15660) and D.H. (DE-FG02-05ER15661). Work at UMBC was supported by U. of Maryland, Baltimore County (start-up funds and SRAIS Award), and the National Science Foundation under CHE-1301109 (M.P.). Work at UConn was supported by the National Science Foundation via grant EMT-0829916 (R.R.B.). Transient absorption studies for the bacteriochlorin dyads in benzonitrile were performed in the Ultrafast Laser Facility of the Photosynthetic Antenna Research Center, an Energy Frontier Research Center funded by the U.S. Department of Energy, Office of Basic Energy Sciences, under Award No. DE-SC0001035. N.N.E. is a member of Meyerhoff Scholars Program at UMBC, supported by NIGMS Initiative for Maximizing Students Development Grant (Grant 2 R25-GM55036).

REFERENCES

- (1) Gueymard, C. A. The Sun's Total and Spectral Irradiance for Solar Energy Applications and Solar Radiation Models. *Sol. Energy* **2004**, *76*, 423–453.
- (2) Scheer, H. In *Chlorophylls and Bacteriochlorophylls. Biochemistry, Biophysics, Functions and Applications*; Grimm, B., Porra, R. J., Rüdiger, W., Scheer, H., Eds.; Advances in Photosynthesis and Respiration; Springer: Dordrecht, The Netherlands, 2006; Vol. 25, pp 1–26.
- (3) Gouterman, M. Optical Spectra and Electronic Structure of Porphyrins and Related Rings. In *The Porphyrins*; Dolphin, D., Ed.; Academic Press: New York, 1978; Vol. 3 pp 1–165.
- (4) Holten, D.; Bocian, D. F.; Lindsey, J. S. Probing Electronic Communication in Covalently Linked Multiporphyrin Arrays. A Guide to the Rational Design of Molecular Photonic Devices. *Acc. Chem. Res.* **2002**, *35*, 57–69.
- (5) Harvey, P. D. In *The Porphyrin Handbook*; Kadish, K. M., Smith, K. M., Guillard, R., Eds.; Academic Press: San Diego, CA, 2003; Vol. 18, pp 63–250.
- (6) Harvey, P. D.; Stern, C.; Guillard, R. In *Handbook of Porphyrin Science*; Kadish, K. M., Smith, K. M., Guillard, R., Eds.; World Scientific Publishing Co.: Singapore, 2011; Vol. 11, pp 1–179.
- (7) Kim, D.; Osuka, A. In *Multiporphyrin Arrays*; Kim, D., Ed; Pan Sanford Publishing Pte. Ltd: Singapore, 2012; pp 1–44.
- (8) Kee, H. L.; Kirmaier, C.; Tang, Q.; Diers, J. R.; Muthiah, C.; Taniguchi, M.; Laha, J. K.; Ptaszek, M.; Lindsey, J. S.; Bocian, D. F.; et al. Effects of Substituents on Synthetic Analogs of Chlorophylls. Part 2: Redox Properties, Optical Spectra and Electronic Structure. *Photochem. Photobiol.* **2007**, *83*, 1125–1143.
- (9) Taniguchi, M.; Cramer, D. L.; Bhise, A. D.; Kee, H. L.; Bocian, D. F.; Holten, D.; Lindsey, J. S. Accessing the Near-Infrared Spectral Region with Stable, Synthetic, Wavelength-Tunable Bacteriochlorins. *New J. Chem.* **2008**, *32*, 947–958.
- (10) Yang, E.; Kirmaier, C.; Krayer, M.; Taniguchi, M.; Kim, H.-J.; Diers, J. R.; Bocian, D. F.; Lindsey, J. S.; Holten, D. Photophysical Properties and Electronic Structure of Stable, Tunable Synthetic Bacteriochlorins: Extending the Features of Native Photosynthetic Pigments. *J. Phys. Chem. B* **2011**, *115*, 10801–10816.
- (11) Faries, K. M.; Diers, J. R.; Springer, J. W.; Yang, E.; Ptaszek, M.; Lahaye, D.; Krayer, M.; Taniguchi, M.; Kirmaier, C.; Lindsey, J. S.; et al. Photophysical Properties and Electronic Structure of Chlorin–Imides: Bridging the Gap Between Chlorins and Bacteriochlorins. *J. Phys. Chem. B* **2015**, *119*, 7503–7515.
- (12) Vairaprakash, P.; Yang, E.; Sahin, T.; Taniguchi, M.; Krayer, M.; Diers, J. R.; Wang, A.; Niedzwiedzki, D. M.; Kirmaier, C.; Lindsey, J. S.; Bocian, D. F.; et al. Extending the Short and Long Wavelength Limits of Bacteriochlorin Near-Infrared Absorption via Dioxo- and Bisimide-Functionalization. *J. Phys. Chem. B* **2015**, *119*, 4382–4395.
- (13) Lin, V. S.-Y.; Dimagno, S. G.; Therien, M. J. Highly Conjugated, Acetylenyl Bridged Porphyrins: New Models for Light-Harvesting Antenna Systems. *Science* **1994**, *264*, 1105–1111.
- (14) Lin, V. S.-Y.; Therien, M. J. The Role of Porphyrin-to-Porphyrin Linkage Topology in the Extensive Modulation of the Absorptive and Emissive Properties of a Series of Ethynyl- and Butadiynyl-Bridged Bis- and Tris(porphinato)zinc Chromophores. *Chem. - Eur. J.* **1995**, *1*, 645–651.
- (15) Kumble, R.; Palese, S.; Lin, V. S.-Y.; Therien, M. J.; Hochstrasser, R. M. Ultrafast Dynamics of Highly Conjugated Porphyrin Arrays. *J. Am. Chem. Soc.* **1998**, *120*, 11489–11498.
- (16) Shediach, R.; Gray, M. H. B.; Uyeda, H. T.; Johnson, R. J.; Hupp, J. T.; Angiolillo, P. J.; Therien, M. J. Singlet and Triplet Excited States of Emissive, Conjugated Bis(porphyrin) Compounds Probed by Optical and EPR Spectroscopic Methods. *J. Am. Chem. Soc.* **2000**, *122*, 7017–7033.
- (17) Duncan, T. V.; Susumu, K.; Sinks, L. E.; Therien, M. J. Exceptional Near-Infrared Fluorescence Quantum Yields and Excited-State Absorptivity of Highly Conjugated Porphyrin Arrays. *J. Am. Chem. Soc.* **2006**, *128*, 9000–9001.
- (18) Duncan, T. V.; Wu, S. P.; Therien, M. J. Ethyne-Bridged (Porphinato)Zinc(II)-(Porphinato)Iron(III) Complexes: Phenomenological Dependence of Excited-State Dynamics upon (Porphinato)Iron Electronic Structure. *J. Am. Chem. Soc.* **2006**, *128*, 10423–10435.
- (19) Duncan, T. V.; Ishizuka, T.; Therien, M. J. Molecular Engineering of Intensely Near-Infrared Absorbing Excited States in Highly Conjugated Oligo(porphinato)zinc-(Polypyridyl)metal(II) Supermolecules. *J. Am. Chem. Soc.* **2007**, *129*, 9691–9703.
- (20) Susumu, K.; Duncan, T. V.; Therien, M. J. Potentiometric, Electronic Structural, and Ground- and Excited-State Optical Properties of Conjugated Bis[(Porphinato)zinc(II)] Compounds Featuring Proquinoidal Spacer Units. *J. Am. Chem. Soc.* **2005**, *127*, 5186–5195.
- (21) Piet, J. J.; Warman, J. M.; Anderson, H. L. Photo-induced Charge Separation on Conjugated Porphyrin Chains. *Chem. Phys. Lett.* **1997**, *266*, 70–74.
- (22) Taylor, P. N.; Wylie, A. P.; Huuskonen, J.; Anderson, H. L. Enhanced Electronic Conjugation in Anthracene-Linked Porphyrins. *Angew. Chem., Int. Ed.* **1998**, *37*, 986–989.
- (23) Piet, J. J.; Taylor, P. N.; Anderson, H. L.; Osuka, A.; Warman, J. M. Excitonic Interactions in the Singlet and Triplet Excited States of Covalently Linked Zinc Porphyrin Dimers. *J. Am. Chem. Soc.* **2000**, *122*, 1749–1757.
- (24) Winters, M. U.; Kärnbratt, J.; Eng, M.; Wilson, C. J.; Anderson, H. L.; Albinsson, B. Photophysics of a Butadiyne-Linked Porphyrin Dimers: Influence of Conformational Flexibility in the Ground and First Singlet Excited State. *J. Phys. Chem. C* **2007**, *111*, 7192–7199.
- (25) Kuimova, M. K.; Hoffmann, M.; Winters, M. U.; Eng, M.; Balaz, M.; Clark, I. P.; Collins, H. A.; Tavender, S. M.; Wilson, C. J.; Albinsson, B.; et al. Determination of the Triplet State Energies of a Series of Conjugated Porphyrin Oligomers. *Photochem. Photobiol. Sci.* **2007**, *6*, 675–682.
- (26) Chang, M.-H.; Hoffmann, M.; Anderson, H. L.; Herz, L. M. Dynamics of Excited-State Conformational Relaxation and Electronic Delocalization in Conjugated Porphyrin Oligomers. *J. Am. Chem. Soc.* **2008**, *130*, 10171–10178.
- (27) Kocherzhenko, A. A.; Patwardhan, S.; Grozema, F. C.; Anderson, H. L.; Siebbeles, L. D. A. Mechanism of Charge Transport along Zinc Porphyrin-Based Molecular Wires. *J. Am. Chem. Soc.* **2009**, *131*, 5522–5529.
- (28) Sedghi, G.; Esdaile, L. J.; Anderson, H. L.; Martin, S.; Bethell, D.; Higgins, S. J.; Nichols, R. J. Comparison of the Conductance of Three Types of Porphyrin-Based Molecular Wires: β , *meso*, β -Fused Tapes, *meso*-Butadiyne-Linked and Twisted *meso-meso* Linked Oligomers. *Adv. Mater.* **2012**, *24*, 653–657.
- (29) Kelley, R. F.; Lee, S. J.; Wilson, T. M.; Nakamura, Y.; Tiede, D. M.; Osuka, A.; Hupp, J. T.; Wasielewski, M. R. Intramolecular Energy Transfer within Butadiyne-Linked Chlorophyll and Porphyrin Dimer-Faced, Self-Assembled Prisms. *J. Am. Chem. Soc.* **2008**, *130*, 4277–4284.
- (30) Sasaki, S.-i.; Mizutani, K.; Kunieda, M.; Tamiaki, H. Synthesis and Optical Properties of C3-Ethynylated Chlorin and π -Extended Chlorophyll Dyads. *Tetrahedron* **2011**, *67*, 6065–6072.
- (31) Jaquinod, L.; Forsyth, T. P.; Smith, K. M.; Senge, M. O.; Pandey, R. K. Planar Bischlorophyll Derivatives with a Completely Conjugated π -System: Model Compounds for the Special Pair in Photosynthesis. *Angew. Chem., Int. Ed. Engl.* **1996**, *35*, 1840–1842.
- (32) Li, G.; Dobhal, M. P.; Graham, A.; Shibata, M.; Zheng, G.; Kozyrev, A.; Pandey, R. K. Thermolysis of *vic*-Dihydroxybacteriochlorins: Effect of the Nature of Substrates in Directing the Formation of Chlorin-Chlorin Dimers with Fixed and Flexible Orientations and Their Preliminary In Vitro Photosensitizing Efficacy. *J. Org. Chem.* **2003**, *68*, 3762–3772.
- (33) Wasielewski, M. R. In *Chlorophylls*; Scheer, H., Ed.; CRC Press: Boca Raton, FL, 1991; pp 269–286.
- (34) Kee, H. L.; Nothdurft, R.; Muthiah, C.; Diers, J. R.; Fan, D.; Ptaszek, M.; Bocian, D. F.; Lindsey, J. D.; Culver, J. P.; Holten, D. Examination of Chlorin-Bacteriochlorin Energy-Transfer Dyads as Prototypes for Near-infrared Molecular Imaging Probes. *Photochem. Photobiol.* **2008**, *84*, 1061–1072.
- (35) Kee, H. L.; Diers, J. R.; Ptaszek, M.; Muthiah, C.; Fan, D.; Lindsey, J. S.; Bocian, D. F.; Holten, D. Chlorin-Bacteriochlorin Energy-transfer Dyads as Prototypes for Near-infrared Molecular Imaging Probes:

Controlling Charge-transfer and Fluorescence Properties in Polar Media. *Photochem. Photobiol.* **2009**, *85*, 909–920.

(36) Lindsey, J. S.; Mass, O.; Chen, C.-Y. Tapping the Near-Infrared Spectral Region with Bacteriochlorin Arrays. *New J. Chem.* **2011**, *35*, 511–516.

(37) Yu, Z.; Pancholi, C.; Bhagavathy, G. V.; Kang, H. S.; Nguyen, J. K.; Ptaszek, M. Strongly Conjugated Hydroporphyrin Dyads: Extensive Modification of Hydroporphyrins' Properties by Expanding the Conjugated System. *J. Org. Chem.* **2014**, *79*, 7910–7925.

(38) Shrestha, K.; González-Delgado, J. M.; Blew, J. H.; Jakubikova, E. Electronic Structure of Covalently Linked Zinc Bacteriochlorin Molecular Arrays: Insights into Molecular Design for NIR Light Harvesting. *J. Phys. Chem. A* **2014**, *118*, 9901–9913.

(39) Diers, J. R.; Tang, Q.; Hondros, C. J.; Chen, C.-Y.; Holten, D.; Lindsey, J. S.; Bocian, D. F. Vibronic Characteristics and Spin-Density Distributions in Bacteriochlorins as Revealed by Spectroscopic Studies of 16 Isotopologues. Implications for Energy- and Electron-Transfer in Natural Photosynthesis and Artificial Solar-Energy Conversion. *J. Phys. Chem. B* **2014**, *118*, 7520–7532.

(40) Except for molecular mechanics and semi-empirical models, the calculation methods used in Spartan '10 have been documented in: Shao, Y.; Molnar, L. F.; Jung, Y.; Kussmann, J.; Ochsenfeld, C.; Brown, S. T.; Gilbert, A. T. B.; Slipchenko, L. V.; Levchenko, S. V.; O'Neill, D. P.; et al. Advances in Methods and Algorithms in a Modern Quantum Chemistry Program Package. *Phys. Chem. Chem. Phys.* **2006**, *8*, 3172–3191.

(41) Kauppinen, J. K.; Moffatt, D. J.; Hollberg, M.; Mantsch, H. Characteristics of the LOMEP Line-Narrowing Method. *Appl. Spectrosc.* **1991**, *45*, 1516–1521.

(42) Kauppinen, J.; Moffatt, D.; Mantsch, H.; Cameron, D. Fourier Self-Deconvolution: A Method for Resolving Intrinsically Overlapped Bands. *Appl. Spectrosc.* **1981**, *35*, 271–276.

(43) Butler, W. L.; Hopkins, D. W. Higher Derivative Analysis of Complex Absorption Spectra. *Photochem. Photobiol.* **1970**, *12*, 439–450.

(44) Allen, L. C.; Gladney, H.; Glarum, S. Resolution Enhancement for Spectra of Chemical and Physical interest. *J. Chem. Phys.* **1964**, *40*, 3135–3141.

(45) Muthiah, C.; Ptaszek, M.; Nguyen, T.; Flack, K. M.; Lindsey, J. S. Two Complementary Routes to 7-Substituted Chlorins. Partial Mimics of Chlorophyll *b*. *J. Org. Chem.* **2007**, *72*, 7736–7749.

(46) Laha, J. K.; Muthiah, C.; Taniguchi, M.; McDowell, B.; Ptaszek, M.; Lindsey, J. S. Synthetic Chlorins Bearing Auxochromes at the 3- and 13-Positions. *J. Org. Chem.* **2006**, *71*, 4092–4102.

(47) Krayer, M.; Ptaszek, M.; Kim, H.-J.; Meneely, K. R.; Fan, D.; Secor, K.; Lindsey, J. S. Expanded Scope of Synthetic Bacteriochlorins via Improved Acid Catalysis Conditions and Diverse Dihydrodipyrin-Acetals. *J. Org. Chem.* **2010**, *75*, 1016–1039.

(48) Yu, Z.; Ptaszek, M. Multifunctional Bacteriochlorins from Selective Palladium-Coupling Reactions. *Org. Lett.* **2012**, *14*, 3708–3711.

(49) Anderson, H. L.; Wylie, A. P.; Prout, K. *meso*-Tetraalkynylporphyrins. *J. Chem. Soc., Perkin Trans. 1* **1998**, *1*, 1607–1611.

(50) Gouterman, M. Study of the Effects of Substitution on the Absorption Spectra of Porphin. *J. Chem. Phys.* **1959**, *30*, 1139–1161.

(51) Gouterman, M. Spectra of Porphyrins. *J. Mol. Spectrosc.* **1961**, *6*, 138–163.

(52) Weiss, C., Jr. The Pi Electron Structure and Absorption Spectra of Chlorophylls in Solution. *J. Mol. Spectrosc.* **1972**, *44*, 37–80.

(53) Petke, J. D.; Maggiora, G. M.; Shipman, L. L.; Christoffersen, R. E. Stereoelectronic Properties of Photosynthetic and Related Systems—VI. *Ab Initio* Configuration Interaction Calculations on the Ground and Lower Excited Singlet and Triplet States of Ethyl Bacteriochlorophyllide-*a* and Ethyl Bacteriopheophorbide-*a*. *Photochem. Photobiol.* **1980**, *32*, 399–414.

(54) Birks, J. B. *Photophysics of Aromatic Molecules*; Wiley-Interscience: London, 1970; pp 142–192.

(55) Felton, R. H. In *The Porphyrins*; Dolphin, D., Ed.; Academic Press: New York, 1978; Vol. V, pp 53–126.

(56) Donohoe, R. J.; Duchowski, J. K.; Bocian, D. F. Hole Delocalization in Oxidized Cerium (IV) Porphyrin Sandwich Complexes. *J. Am. Chem. Soc.* **1988**, *110*, 6119–6124.

(57) Bilsel, O.; Rodriguez, J.; Milam, S. N.; Gorlin, P. A.; Girolami, G. S.; Suslick, K. S.; Holten, D. Electronic States and Optical Properties of Porphyrins in van der Waals Contact: Th^{IV} Sandwich Complexes. *J. Am. Chem. Soc.* **1992**, *114*, 6528–6538.

(58) Kasha, M.; Rawls, H. R.; Ashraf El-Bayoumi, M. The Exciton Model in Molecular Spectroscopy. *Pure Appl. Chem.* **1965**, *11*, 371–392.

(59) Linnanto, J.; Korppi-Tommola, J. Quantum Chemical Simulation of Excited States of Chlorophylls, Bacteriochlorophylls and Their Complexes. *Phys. Chem. Chem. Phys.* **2006**, *8*, 663–687.

(60) Petit, L.; Quartarolo, A.; Adamo, C.; Russo, N. Spectroscopic Properties of Porphyrin-Like Photosensitizers: Insights from Theory. *J. Phys. Chem. B* **2006**, *110*, 2398–2404.

(61) Johnson, S. G.; Svec, W. A.; Wasielewski, M. R. Solvent Polarity Dependent Photophysics of a Fixed-Distance, Symmetric Chlorophyll Dimer. A Model of the Special Pair in Photosynthetic Reaction Centers. *Isr. J. Chem.* **1988**, *28*, 193–203.

(62) Johnson, S. G.; Small, G. J.; Johnson, D. G.; Svec, W. A.; Wasielewski, M. R. Temperature and Solvent-Polarity Dependence of the Absorption and Fluorescence Spectra of a Fixed-Distance Symmetric Chlorophyll Dimer. *J. Phys. Chem.* **1989**, *93*, 5437–5444.

(63) McDowell, L. M.; Kirmaier, C.; Holten, D. Charge Transfer and Charge Resonance States of the Primary Electron Donor in Wild-Type and Mutant Bacterial Reaction Centers. *Biochim. Biophys. Acta, Bioenerg.* **1990**, *1020*, 239–246.

(64) Thompson, M. A.; Zerner, M. C.; Fajer, J. Electronic Structure of Bacteriochlorophyll Dimers. Bacteriochlorin Models. *J. Phys. Chem.* **1990**, *94*, 3820–3828.

(65) Warshel, A.; Parson, W. W. Spectroscopic Properties of Photosynthetic Reaction Centers. I. Theory. *J. Am. Chem. Soc.* **1987**, *109*, 6143–6152.

(66) Zhang, L. Y.; Friesner, R. A. *Ab Initio* Calculation of Electronic Coupling in the Photosynthetic Reaction Center. *Proc. Natl. Acad. Sci. U. S. A.* **1998**, *95*, 13603–13605.

NOTE ADDED AFTER ASAP PUBLICATION

This paper was published ASAP on January 14, 2016, with an incorrect version of Scheme 1. The corrected version was reposted on January 19, 2016.